

## Beyond scratching the surface : intrinsic tribological performance of polymers

**Citation for published version (APA):**

Schaake, R. P. (2006). *Beyond scratching the surface : intrinsic tribological performance of polymers*. [Phd Thesis 1 (Research TU/e / Graduation TU/e), Mechanical Engineering]. Technische Universiteit Eindhoven. <https://doi.org/10.6100/IR611948>

**DOI:**

[10.6100/IR611948](https://doi.org/10.6100/IR611948)

**Document status and date:**

Published: 01/01/2006

**Document Version:**

Publisher's PDF, also known as Version of Record (includes final page, issue and volume numbers)

**Please check the document version of this publication:**

- A submitted manuscript is the version of the article upon submission and before peer-review. There can be important differences between the submitted version and the official published version of record. People interested in the research are advised to contact the author for the final version of the publication, or visit the DOI to the publisher's website.
- The final author version and the galley proof are versions of the publication after peer review.
- The final published version features the final layout of the paper including the volume, issue and page numbers.

[Link to publication](#)

**General rights**

Copyright and moral rights for the publications made accessible in the public portal are retained by the authors and/or other copyright owners and it is a condition of accessing publications that users recognise and abide by the legal requirements associated with these rights.

- Users may download and print one copy of any publication from the public portal for the purpose of private study or research.
- You may not further distribute the material or use it for any profit-making activity or commercial gain
- You may freely distribute the URL identifying the publication in the public portal.

If the publication is distributed under the terms of Article 25fa of the Dutch Copyright Act, indicated by the "Taverne" license above, please follow below link for the End User Agreement:

[www.tue.nl/taverne](http://www.tue.nl/taverne)

**Take down policy**

If you believe that this document breaches copyright please contact us at:

[openaccess@tue.nl](mailto:openaccess@tue.nl)

providing details and we will investigate your claim.

# **Beyond scratching the surface**

*Intrinsic tribological performance of polymers*

CIP-DATA LIBRARY TECHNISCHE UNIVERSITEIT EINDHOVEN

Schaake, Richard P.

Beyond scratching the surface : Intrinsic tribological performance  
of polymers / by Richard P. Schaake. - Eindhoven :  
Technische Universiteit Eindhoven, 2006.

A catalogue record is available from the Library Eindhoven University of Technology

ISBN-10: 90-386-2778-5

ISBN-13: 978-90-386-2778-6

Trefwoorden: Polymer Friction, Polymer Wear, Polystyrene (PS), Polyethylene (PE),  
Molecular weight, Single-Asperity [5mm]

Reproduction: University Press Facilities, Eindhoven, The Netherlands.

Cover design: Paul Verspaget.

Cover illustration: Richard Schaake

# **Beyond scratching the surface**

*Intrinsic tribological performance of polymers*

PROEFSCHRIFT

ter verkrijging van de graad van doctor aan de  
Technische Universiteit Eindhoven, op gezag van de  
Rector Magnificus, prof.dr.ir. C.J. van Duijn, voor een  
commissie aangewezen door het College voor  
Promoties in het openbaar te verdedigen  
op donderdag 7 september 2006 om 16.00 uur

door

**Richard Pieter Schaake**

geboren te Apeldoorn

Dit proefschrift is goedgekeurd door de promotoren:

prof.dr.ir. H.E.H. Meijer

en

prof.dr.ir. J.M.J. den Toonder

Copromotor:

dr.ir. W.P. Vellinga





# Contents

---

<b>Summary</b>	<b>xi</b>
<b>1 Introduction</b>	<b>1</b>
1.1 The Amontons–Coulomb law . . . . .	1
1.2 Contact Mechanics . . . . .	2
1.3 Intrinsic behaviour of polymers . . . . .	3
1.4 Survey of the thesis . . . . .	4
References . . . . .	5
<b>2 Single–asperity tribology, the LFA</b>	<b>7</b>
2.1 Introduction . . . . .	7
Single–asperity techniques . . . . .	7
2.2 General information about the LFA . . . . .	8
Components of the LFA . . . . .	8
2.3 Motion . . . . .	10
Principle . . . . .	10
Velocity . . . . .	10
Position . . . . .	11
Rapid deceleration . . . . .	11
Other sources of errors . . . . .	13
2.4 Force measurement . . . . .	14
Principle . . . . .	14
Measurement range and accuracy . . . . .	14
2.5 Tips . . . . .	15
Tips for the LFA . . . . .	15
What is a single–asperity tip? . . . . .	15
Diamond tips . . . . .	16
Tips obtained by wire etching . . . . .	17
Other possibilities for obtaining tips . . . . .	18
2.6 Operation . . . . .	18



	Leafspring unit preparation . . . . .	18
	Calibration . . . . .	20
	Experiments . . . . .	21
2.7	Conclusion . . . . .	21
	References . . . . .	22
<b>3</b>	<b>Velocity dependence of friction on polystyrene (PS)<sup>1</sup></b>	<b>23</b>
3.1	Introduction . . . . .	23
	Friction dynamics . . . . .	23
	Friction on polystyrene . . . . .	24
	Rate-and-state approach . . . . .	25
	Slide-hold-slide experiments . . . . .	26
3.2	Materials and method . . . . .	27
	Materials . . . . .	27
	Slide-indent-slide experiments . . . . .	27
3.3	Results and discussion . . . . .	29
	Dynamic friction . . . . .	29
	Static Contacts . . . . .	30
	Rate-and-state interpretation . . . . .	34
	Conclusion . . . . .	35
	References . . . . .	37
<b>4</b>	<b>Molecular weight dependence of polyethylene (PE) wear<sup>1</sup></b>	<b>39</b>
4.1	Introduction . . . . .	39
	Application of PE in tribological contacts . . . . .	39
	Wear of polyethylene . . . . .	40
	Influence of molar mass on processing and wear . . . . .	41
	Wear measurement methods . . . . .	43
	Aim of this study . . . . .	45
4.2	Materials and method . . . . .	45
	Materials . . . . .	45
	Method . . . . .	46
4.3	Results . . . . .	50
	Development of the method . . . . .	50
	Results obtained using the method developed . . . . .	55
4.4	Conclusion . . . . .	59
	References . . . . .	60
<b>5</b>	<b>Conclusions and recommendations</b>	<b>63</b>
5.1	Conclusions . . . . .	63
5.2	Recommendations . . . . .	64

<b>Samenvatting</b>	<b>67</b>
<b>Dankwoord</b>	<b>69</b>
<b>Curriculum Vitae</b>	<b>71</b>
<b>List of publications by Richard Schaake</b>	<b>73</b>



# Summary

---

Quantifying and understanding friction and wear behaviour of any type of material remains a challenge to this day. This is also true for polymers that are used frequently in sliding applications. This thesis focuses on the development of quantitative measurement techniques that can be used to understand friction and wear of polymers.

To understand the influence of material properties on friction and wear behaviour it is necessary to zoom in on the relevant processes in a sliding contact. A macroscopic contact between two surfaces typically consists of multiple contacts between roughness peaks. These micro-contacts make up the real contact area which is usually a small fraction of the apparent contact area, and which depends on the mechanical properties of both surfaces as well as on the loading conditions. The friction force measured in experiments is the product of this real contact area and an average effective shear stress.

Because the real contact area is difficult to control and measure for macroscopic contacts such contacts are not very useful in separating the contributions to the friction force. In contrast, single asperity techniques offer the possibility to control independently the contact area and normal load and therefore offer a way forward to a critical interpretation of measured friction forces.

In the work described in this thesis microscopic tribological single-asperity experiments are used to study structure-property relations. These single asperity experiments are performed using the Lateral Force Apparatus that was drastically modified to better suit this purpose. A new driving system was developed that allows friction measurements in which the sliding velocity may be varied across 5 orders of magnitude with accurate position control. This combination makes it possible to perform single-asperity measurements at widely differing speeds which are shown to be important for the interpretation of sliding friction on polymers. Accurate position control is shown to be crucial in developing advanced wear measurement techniques.

In sliding friction distinction between the contribution of contact area and effective

shear stress to the friction force is a key issue. Depending on mechanical properties and loading conditions, all materials exhibit creep on a characteristic time scale. In polymers creep is especially relevant since the associated timescales are relatively short. In single asperity friction the asperity radius and sliding speed set a contact time, during which the contact area may evolve by creep. It is shown that the contributions of contact area and effective shear stress can be distinguished from one another using single-asperity measurements at widely differing sliding velocities.

In the study of wear the interpretation of measurements on macroscopic multi-asperity contacts also pose problems since they consist of a collection of micro-contacts between deformed asperities. Since the strain at failure of a polymer is expected to be an important factor in determining the wear of polymers the unambiguous strain distribution of a single asperity contact is an advantage in the study of structure-wear relations.

In this thesis a novel single-asperity technique to measure wear rate is developed. In this method the wear rate is measured in real time. The method is fast, uses very little material, and yet gives good statistics and a strong correlation with macroscopically measured wear rates. In a study on PE it is found that the wear rate is related to the molecular weight.

Quantitative single-asperity measurements are a critical step in understanding structure-tribology relations. While macroscopic tribological experiments can only scratch the surface of structure-tribology relations, single-asperity techniques probe the material properties lying underneath.

## CHAPTER ONE

# Introduction

---

'If we were like computers, we'd be able to copy our minds to children, so that they would grow up agreeing with every opinion that we hold dear. Well, actually they wouldn't, though they might start out that way. There is an aspect to education that we want to draw to your attention. We call it 'lies-to-children'...'

'...The early stages of education have to include a lot of lies-to-children, because early explanations have to be simple. However, we live in a complex world, and lies-to-children must eventually be replaced by more complex stories if they are not to become delayed-action genuine lies.'

– Terry Pratchett, Ian Stewart and Jack Cohen: The Science of Discworld [1]

### 1.1 The Amontons–Coulomb law

In 1699 Amontons described his friction experiments. He made two important statements:

- 1) Friction force is proportional to load.
- 2) The dissipative mechanism can be caused by moving roughness peaks over one another and by wear or deformation of either surface.

In 1750 Euler made a distinction between static and dynamic friction, stating that the friction force that needs to be overcome in order to set a contact in motion is greater than the friction force acting on a sliding contact. He explained this with roughness peaks interlocking when a contact is in rest, requiring a larger force to lift the interlocking roughness peaks from their valleys. In 1773 Coulomb added that

friction is independent of sliding velocity. These observations form the basis for what has become commonly known as the Amontons–Coulomb law:

$$F_F = \mu F_N \quad (1.1)$$

Where  $F_F$  is the friction force,  $F_N$  the normal force and  $\mu$  a constant which has become known as the coefficient of friction.

In 1882 Hertz' ground breaking paper on the contact between elastic spheres [2] offered a foothold for the study of another dissipative mechanism than Euler's suggestion of interlocking roughness peaks, namely the irreversible deformation of roughness peaks. The study of this deformation mechanism has become known as contact mechanics.

## 1.2 Contact Mechanics

In 1954 Bowden and Tabor introduced the concept of asperities [3,4], a convenient method to handle contact mechanical friction. This concept has dominated the developments in this field since. They stated that the friction force is determined by a real contact area, which in turn is determined by the deformation of asperities. According to their asperity concept, the contact between two rough metal surfaces has a real area of contact. They argue that under certain simplifying assumptions the real contact area of a multi-asperity contact is proportional to the normal load. This means that the effective shear stress acting on the asperities is independent of normal load and the Amontons–Coulomb law can be rewritten as:

$$F_F = \bar{\sigma}_s \Sigma_A \quad (1.2)$$

with  $\bar{\sigma}_s$  the average shear stress acting on the cumulative contact area of all micro contacts,  $\Sigma_A$ . This approach offers an opportunity to relate friction to material properties. The contact area is determined by the mechanical behaviour of the asperities under compression and the shear stress by the shear behaviour of the interface.

The formulation is robust. It offers an explanation for the Amontons–Coulomb law and provides a possible explanation for contacts where the Amontons–Coulomb law fails. Most importantly it doesn't a priori exclude the existence of influences on friction force besides the normal force. When the Amontons–Coulomb law fails, either the shear stress or the total, or real, contact area is dependent on the sliding conditions, e.g. sliding velocity [5]. The main reason why Bowden and Tabor's description, equation 1.2, has not fully made the Amontons–Coulomb law obsolete is that the real contact area can only be measured in a limited amount of macroscopic contacts, while the shear stress can not be measured at all, it must be calculated by dividing the friction force by the real contact area.

Another concept, developed parallel to Bowden and Tabor's asperity concept, is the concept of protuberances from Archard [6], it has long been more or less ignored. In

the protuberance concept the contact area is never fully proportional to the normal force, but rather a via power law relation between contact area and normal force, where the power increases towards 1 with an increasing number of micro-contacts. This approach offers a basis to describe friction in macroscopic contacts where the relation between contact area and normal force is non-linear, it also explains why very small asperities on a rough surface may not affect the contact area significantly.

In fundamental tribological research, contact mechanics has become invaluable. Research focussing on the effects of material properties on tribological performance, see e.g. [7–11], is only successful if results are obtained in such a manner that a quantification of the contact area is possible. In order to *quantitatively* relate tribological performance and material properties using contact mechanics the contact geometry needs to be kept as simple as possible. This can be achieved by using single-asperity techniques, see e.g. [12,13].

Single-asperity techniques are especially effective because they offer a way to experimentally access the contact mechanics. Instead of a distribution of contacts forming a total contact area,  $\Sigma_A$ , that is proportional to the normal load,  $F_N$ , single-asperity contacts give only a single contact area,  $A_c$ . Depending on the contact geometry the contact area,  $A_c$ , is not proportional to the normal load,  $F_N$ , but follows a power-law function of the normal load instead [6,14]. E.g. a contact between elastic spheres shows a proportionality between  $A_c$  and  $F_N^{2/3}$ . This unique relation between  $A_c$  and  $F_N$  allows for a contact-mechanical approach of friction studies, even when the contact area cannot be measured directly, e.g. [15].

In contacts between rough surfaces the local deformations and forces may vary a lot, effectively limiting the study of shear stress effects to a statistical approach while extremes may be just as relevant as averages. Apart from this, changes in the contact situation due to frictional heat, chemical reactions, and a constantly changing contact geometry due to wear and deformation further complicate an effective use of a contact mechanical approach for applied friction studies. All these factors effectively made the Amontons–Coulomb law a powerful and efficient *lie-to-children* in the education of engineers.

## 1.3 Intrinsic behaviour of polymers

The intrinsic properties of polymers as measured during homogeneous deformation can be very different from the macroscopic behaviour as measured in tension. The intrinsic properties are properties inherent to the chains that constitute the polymer. For example, polystyrene (PS) is known as a brittle material which typically breaks at tensile strains of a few percent, while polycarbonate (PC) is known for its high toughness (bullet-proof glass). However, PS is intrinsically very tough; its flexible backbone and low entanglement density allow the coiled chain to stretch to a large extent, while the stiffer, more entangled, PC can achieve only smaller local strains [16]. The difference in ductility between PS and PC is caused by differences in resistance to



strain localisation [17]. The entanglement network serves to transfer strains. The more unstable strain localisation occurring in PS manifests itself as crazing. Inside these crazes chains are stretched to their breaking point, but the strain keeps localised in the plane of the craze. The more entangled PC localises its strain in a neck region, but strain hardening causes a neck to form, which finally extends through the total sample.

Interestingly strain localisation is only an issue in tensile loading. Under compression strain localisation does not occur and the intrinsic material properties are utilised. Polymer behaviour under tribological loading, which is determined by the materials compressive and shear behaviour, is therefore expected to be determined by the polymers' intrinsic properties to a large extent.

## 1.4 Survey of the thesis

The focus of this thesis is the development of experimental methods for studying the relation between intrinsic properties of polymers and their performance under tribological loading. This requires a well-defined mechanical loading situation.

Experiments with well-defined geometries allow for a direct and quantitative measurement of contact-mechanics on a polymer. Particularly in nanometre sized contacts, single-asperity tribology on polymers has become more common over the last decade [18–20]. However, the micro-scale, relevant to multi-asperity contacts [10], has received relatively little attention from a single-asperity point of view.

The work in this thesis was performed using the Lateral Force Apparatus (LFA). This device is described in detail in chapter 2. Its unique features and accuracy are elucidated. An analysis of the sources of experimental errors is given, as well as how these errors were minimised in the experiments described here.

The rate-dependence of polystyrene friction was examined using a combination of slide-hold-slide experiments and analysis using rate-and-state contact mechanical models. This is the focus of chapter 3. This approach provides a useful tool to characterise the time-dependent aspects of the polymer's mechanical properties when tribologically loaded. The results were compared with those reported in the literature based on experiments performed on macroscopic multi-asperity contacts and nanoscopic single-asperity contacts.

The aspect of polymer wear are described in chapter 4. A single-asperity wear experiment was designed that allows for a quantitative and qualitative study of the wear of polyethylene on a single-asperity level. The wear-rates measured by using the LFA were compared to micro-abrader results from literature.

Finally in chapter 5 conclusions and recommendations for future research are given.

## References

- [1] Pratchett, T., Stewart, I. and Cohen, J. (1999). *The Science Of Discworld*. Ebury Press.
- [2] Hertz, H. (1882). On the contact of elastic solids. *J. Reine Angew. Math.*, **92**, 156–171.
- [3] Bowden, F. P. and Tabor, D. (1954). *The friction and lubrication of solids; Part I*. Clarendon Press, Oxford, United Kingdom, 2nd edition.
- [4] Bowden, F. P. and Tabor, D. (1964). *The friction and lubrication of solids; Part II*. Clarendon Press, Oxford, United Kingdom, 2nd edition.
- [5] Dieterich, J. H. (1978). Time-dependent friction and the mechanics of stick-slip. *PAGEOPH*, **116**, 790–806.
- [6] Archard, J. F. (1957). Elastic deformation and the laws of friction. *Proc. Roy. Soc. A*, **243**, 190–205.
- [7] Mergler, Y. J., van Kampen, R. J., Nauta, W. J., Schaake, R. P., Raas, B., van Griensven, J. G. H. and Meesters, C. M. J. (2004). Influence of yield strength and toughness on friction and wear of polycarbonate. *Wear*, **258**, 915–923.
- [8] Yang, A. C.-M. and Wu, T. W. (1993). Abrasive wear and craze breakdown in polystyrene. *J. Mat. Sci.*, **28**, 955–962.
- [9] Mergler, Y. J. and Huis in 't Veld, A. J. (2003). Micro-abrasive wear of semi-crystalline polymers. In Dalmaz, G. Lubrecht, A., editors, *Tribological Research and Design for Engineering Systems: Proceedings of the 29th Leeds–Lyon Symposium on Tribology held In Leeds, UK 3rd–6th September 2002*, Tribology and Interface Engineering Series, pages 165–173, Amsterdam, 2003. Elsevier.
- [10] Baumberger, T., Berthoud, P. and Caroli, C. (1999). Physical analysis of the state- and rate-dependent friction law. ii. dynamic friction. *Phys. Rev. B*, **60**, 3928–3939.
- [11] Berthoud, P., Baumberger, T., G'Sell, C. and Hiver, J. M. (1999). Physical analysis of the state- and rate-dependent friction law: Static friction. *Phys. Rev. B*, **59**, 14313–14327.
- [12] Gotsmann, B. and Dürig, U. (2004). Thermally activated nanowear modes of a polymer surface induced by a heated tip. *Langmuir*, **20**, 1495–1500.
- [13] Bles, M. H., Winkelman, G. B., Balkenende, A. R. and den Toonder, J. M. J. (2000). The effect of friction on scratch adhesion testing: application to a sol-gel coating on polypropylene. *Thin Sol. Films*, **359**, 1–13.
- [14] Persson, B. N. J. (2000). *Sliding Friction Physical Principles and Applications*. NanoScience and Technology. Springer Verlag, Berlin, 2nd edition.
- [15] Johnson, K. L. (1997). A continuum mechanics model of adhesion and friction in a single asperity contact. In Bhushan, B., editor, *Micro/nanotribology and its applications*, pages 151–168. Kluwer Academic Publishers.
- [16] Kramer, E. J. (1983). Microscopic and molecular fundamentals of crazing. *Adv. Polym. Sci.*, **52–53**, 1–56.
- [17] van Melick, H. G. H., Govaert, L. E. and Meijer, H. E. H. (2003). Localisation phenomena in glassy polymers: influence of thermal and mechanical history. *Polymer*, **44**, 3579–3591.

- [18] Aoike, T., Yamamoto, T., Uehara, H., Yamanobe, T. and Komoto, T. (2001). Surface deformation properties of polystyrene as evaluated from the morphology of surfaces scratched by using the tip of a scanning force microscope. *Langmuir*, **17**, 5688–5692.
- [19] Komvopoulos, K., Do, V., Yamaguchi, E. S. and Ryason, P. R. (2004). Nanomechanical and nanotribological properties of an antiwear tribofilm produced from phosphorus-containing additives on boundary-lubricated steel. *J. of Tribol.*, **126**, 775–780.
- [20] Kajiyama, T., Tanaka, K., Satomi, N. and Takahara, A. (1998). Surface relaxation process of monodisperse polystyrene film based on lateral force microscopic measurements. *Macromolecules*, **31**, 5150–5151.

# Single-asperity tribology, the LFA

---

## 2.1 Introduction

### Single-asperity techniques

Single-asperity techniques have been popular for a long time. The first experiments were in lubrication engineering using a Scanning Force Apparatus (SFA) in which two sheets of atomically flat mica were slid across one another in a medium. This was still at a large scale. Another successful measurement technique is the SFA, a device working on a much larger scale.

Today, single-asperity techniques are mostly associated with Atomic Force Microscopy (AFM), often referred to as Friction Force Microscopy (FFM) when used in the friction mode. The standard FFM has a built in disadvantage that only one laser beam is used to measure both normal and lateral forces, resulting in a relatively large cross-talk between both measurements. Dedicated cantilever constructions, with high stiffness ratios and multiple laser beams have been designed to address this cross-talk problem [1–4].

Different single-asperity techniques make use of a range of scientific instruments to study different aspects of tribology. AFM/FFM and similar techniques are useful to study molecular scale phenomena. Individual relaxation mechanisms can be identified [5,6]. With special cantilever designs even pN forces can be measured [6].

On a scale comparable to that of SFA's, JKR (Johnson–Kendall–Robertson [7]) measurement devices have been developed; such devices are designed to measure adhesive effects. The Lateral Force Apparatus (LFA) works in the  $\text{mN}/\mu\text{m}$  range, a range which has been shown to be relevant in macroscopic multi-asperity contacts involving polymers [8]. Amongst its unique features are the low cross-talk of typically 1% and the large range of sliding velocities that can be achieved. Mark I of this

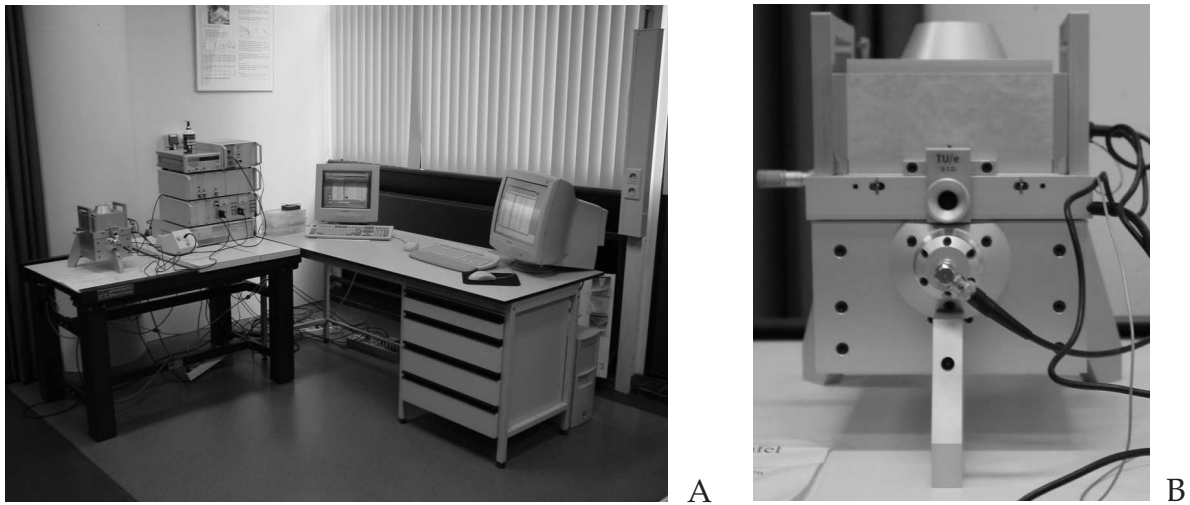


**Figure 2.1:** The LFA Mark II. A) Overview of the LFA and peripheral equipment. B) The core of the LFA, containing the motion stage and force measurement head.

apparatus has been described in [9]. It has since been improved to allow for a large range of sliding velocities combined with an accurate positioning. In this chapter, a description is given of the features, possibilities and accuracy of the LFA Mark II depicted in figure 2.1.

## 2.2 General information about the LFA

### Components of the LFA

A schematic representation of the LFA is given in figure 2.2. The force measurement part has been previously described in [9], and only a short summary is given here. Forces are probed using a calibrated double parallel leafspring unit, the resulting deflection of both lateral and normal force leaf springs is measured using a focus error detection method. The design of the leaf spring unit results in a low cross talk between normal and lateral force measurement, between 0.5% and 5%, depending on the aspect ratio of the leaf springs [9]. The motion in the normal direction is generated by a PI-controlled piezo actuator with a maximum extension of  $45\mu\text{m}$  [9]. A PI feedback system operates during sliding and keeps the normal force constant.

A linear induction motor was designed that ensures a smooth motion of the sample stage, the position and velocity of which are measured independently. The maximum displacement of the stage is 4 mm. The sensitivity for the driving system is adjustable. The motor is operated in a closed PID loop that allows velocity as well as position control of the lateral motion. Complicated velocity vs. time protocols can be programmed.

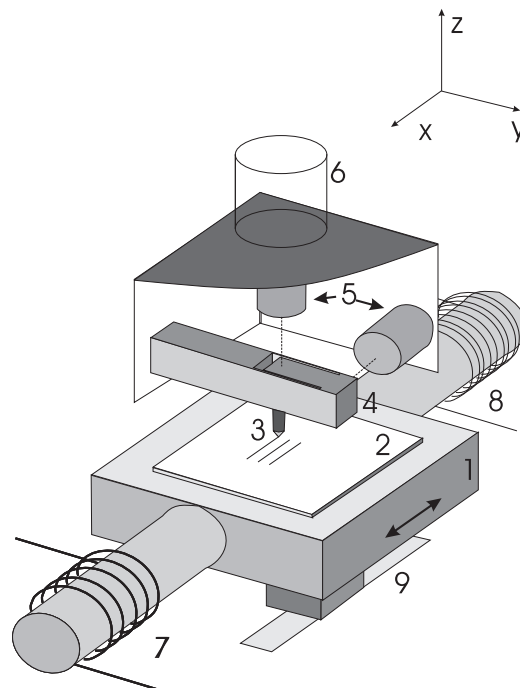


**Figure 2.2:** Schematic representation of the LFA. A tip (3) mounted onto a compact double parallel leaf spring unit (4) slides on a sample (2) mounted onto a sample stage (1). The sample stage is positioned on the moving magnet of a linear induction motor. A coil with thick windings (7) is used to generate the necessary power. The velocity is measured by induction in a second (8) coil, with many windings for sensitivity. The deflections of a calibrated parallel leaf spring unit are measured using focus error detection (5). So in contrast to typical FFM measurements, displacements rather than angular deflections are measured. The deflection in the  $z$  direction is fed into a PID loop that controls to a piezo actuator (6) to maintain a constant normal force. The position of the sample stage is measured using a Heidenhain linear scale (9).

The velocity of the stage is measured independently with a sensitive pick-up coil. This avoids differentiation of the position signal, see below. Measurements of the velocity over five orders of magnitude can be obtained.

The position of the stage is measured with a Heidenhain LIP 382 linear scale, which uses an interferometric method to measure the relative displacement of a diffraction grating fixed to the sample stage with respect to a diffraction grating fixed to the scale. In the current design, where the maximum displacement of the stage is limited to 4 mm, an accuracy 72 nm/mm can be achieved from a reference point determined with 1 nm accuracy.

A 12 bit A/D conversion is used for the velocity, position and force (lateral and normal) signals, for which a number of sensitivity ranges can be set.

## 2.3 Motion

### Principle

The motion of the linear electromagnetic drive is controlled through a feedback loop with a linear electromagnetic tachometer and an optical linear scale. Each of these two devices can be switched on or off as part of the feedback loop under certain trigger conditions.

In the description of the performance of the driving system a distinction is made between measurement of the actual velocity and position, and of the error with respect to programmed velocity and position trajectories. The experiments were carried out using combined velocity and position control or using velocity control only.

### Velocity

Figure 2.3 shows the distribution of measured velocities for target velocities set to 0 nm/s and 10 nm/s, measured with velocity control only. The  $2\sigma$  error on the signal at 0 nm/s is 5.6 nm/s, while at 10 nm/s, it is 4.3 nm/s. This means that 10 nm/s is the minimum possible driving velocity that can be distinguished from stand still.

Across the driving velocity range, 4 separate ranges can be identified to describe the deviation from a set velocity, see table 2.1. These deviations were determined for situations where both position and velocity control were used,  $dv_{pv}$ , and for situations where only velocity control was used,  $dv_v$ . At extremely low driving velocities ( $v < 100\text{nm/s}$ ) the error is determined by the scatter caused by vibrations and expressed as an absolute error. At low velocities ( $100\text{ nm/s} < v < 1\mu\text{m/s}$ ) the error is up to 6% of the full measurement scale. This is also the optimum error that can be achieved at higher driving velocities. However, at medium driving velocities ( $1\mu\text{m/s} < v < 25\mu\text{m/s}$ ) position control will interfere with the accuracy of the driving velocity. Depending on the PID settings the error can increase up to

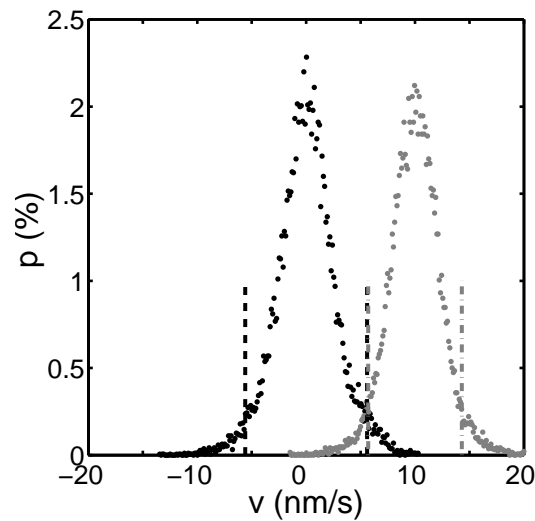


**Figure 2.3:** Probability distribution of measured velocities for target velocities of 0 nm/s and 10 nm/s. A velocity of 10 nm/s can be distinguished from 0 nm/s, as indicated by the coinciding  $2\sigma$  errors (vertical lines).

25% of the full measurement range when position control is used. At high velocities ( $v > 25\mu\text{m/s}$ ) the effect of error induced by position control is always less than 6% of the full measurement scale.

## Position

To investigate the precision with which programmed trajectories are reproduced, the stage was moved across a certain distance at various driving velocities across the four velocity ranges identified in the previous paragraph. A velocity profile was used with high acceleration and deceleration rates and a constant velocity. The sliding distance was dependent on the sliding velocity. The deviation from the position set point was determined using both velocity and position control,  $dx_{pv}$ , and using velocity control only,  $dx_v$ , see table 2.2. The typical error,  $dx_{pv}$  is below 8% of the sliding distance from a reference point when both position and velocity control are used. When only velocity control is used large deviations occur below driving velocities of  $v = 1\mu\text{m/s}$ . Within the medium driving velocity range ( $1\mu\text{m/s} < v < 25\mu\text{m/s}$ ) the deviation from the position set point can be larger, up to 12% of the distance from the reference point.

## Rapid deceleration

One issue regarding the positioning of the stage occurs at rapid deceleration from medium and high sliding velocities. The stage shows a lag with regard to the displacement set point. Instead of decreasing to 0 nm/s as rapidly as possible, the



#	Velocity range	$dv_{pv}$	$dv_v$
1	< 100 nm/s	2.5 nm/s	5 nm/s
2	100 nm/s - 1 $\mu$ m/s	< 6%	< 6%
3	1 $\mu$ m/s - 25 $\mu$ m/s*	6 – 25%	< 6%
4	> 25 $\mu$ m/s	< 6%	< 6%

**Table 2.1:** Difference between measured velocity and the velocity set-point for four ranges: extremely low velocities (1), low velocities (2), medium velocities (3) and high velocities (4). These errors are shown for situations where both position and velocity control are used ( $dv_{pv}$ ) and for those where only velocity control is used ( $dv_v$ ). At very low velocities the error is absolute, determined by vibrations and the resolution of the transducers, while at higher velocities the error is dependent on the signal amplification and is given as an error relative to the full measurement scale. \*The exact limits of the medium velocity range depend on the PID settings, the given values indicate the most extreme limits.

#	Velocity range	$dx_{pv}$	$dx_v$
1	< 100 nm/s	< 8%	> 60%
2	100 nm/s - 1 $\mu$ m/s	< 8%	8 – 60%
3	1 $\mu$ m/s - 25 $\mu$ m/s*	8 – 12%	2 – 8%
4	> 25 $\mu$ m/s	1%	2.5%

**Table 2.2:** Inaccuracy of positioning categorized in four ranges: extremely low velocities (1), low velocities (2), medium velocities (3) and high velocities (4). These inaccuracies are shown for situations where both position and velocity control are used ( $dx_{pv}$ ) and for those where only velocity control is used ( $dx_v$ ). The error is given as an error relative to the desired position after motion in one direction. \*The exact limits of the medium velocity range depend on the PID settings, the given values indicate the most extreme limits.

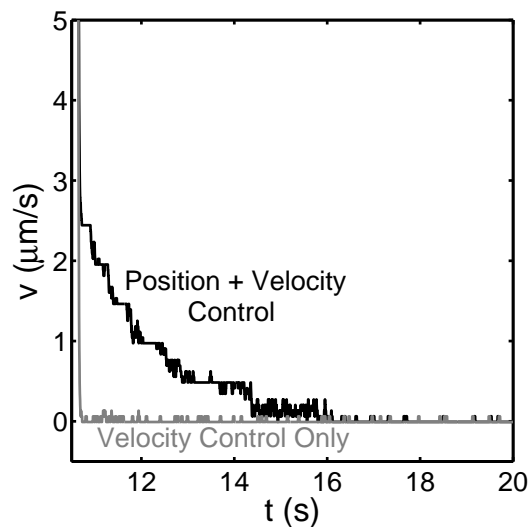


**Figure 2.4:** Driving velocity,  $v$ , at rapid deceleration from  $v = 1 \text{ mm/s}$  to  $v = 0 \text{ nm/s}$ , as a function of time,  $t$ , when both position and velocity control are used (black line) and when only position control is used (grey line).

position control reduces the sliding velocity gradually until the desired position is reached, see figure 2.4.

To allow for experiments that require fast deceleration, such as the slide-indent-slide experiments shown in chapter 3, position control can be used only for low driving velocities. The driving velocity above which the position control is switched off can be adjusted. This way rapid deceleration can be achieved while position drift at stand still is prevented.

## Other sources of errors

It is emphasized that regardless of the precision with which the stage follows the prescribed motion, the actual position and speed of the stage are always measured and ensure unambiguous results. The accuracy of the position measurement turns out to be limited by mechanical noise to about 10 nm (for small displacements), or by the resolution of the A/D conversion (for displacements larger than about 40 microns).

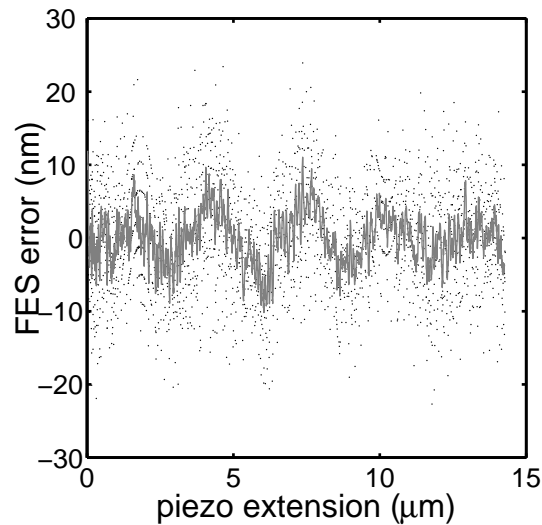


Figure 2.5: Representative measurement of noise on  $z$ -direction FES signal.

## 2.4 Force measurement

### Principle

The force measurement uses focus error detection of parallel double leafspring deflection. This method has the advantage that the sensitive detectors can be placed at a large distance from the tip and cantilever leafsprings. The unique feature of the LFA is that the deflection of the two sets of leafsprings is measured using two focus error detectors. The leafsprings have a high torsional stiffness. Combined with their perpendicular placement this causes a low cross talk between lateral and normal force measurement. Deflection measurement and cross talk have to be calibrated every time a new leafspring unit is mounted, see section 2.6.

### Measurement range and accuracy

The maximum leafspring deflection that can be measured is  $15 - 20\mu\text{m}$ , depending on the alignment of the leafspring unit. Misalignment of the leafspring unit will cause the laser spot to be off the photo diode centre, resulting in a reduced sensor accuracy and increased measurement range [10]. The leafspring  $z$ -deflection can be measured within an accuracy of several tens of nanometres, see figure 2.5. The  $x$ -direction FES signal is typically less accurate since its calibration is more sensitive to mechanical vibrations. The accuracy in the  $x$ -direction is typically around  $100\text{ nm}$ . The laser light has a wavelength  $\lambda \approx 800\text{ nm}$ . At low light intensities, interference can cause a noise of  $1/4$ ,  $1/2$  and  $1\lambda$  on the deflection measurement.

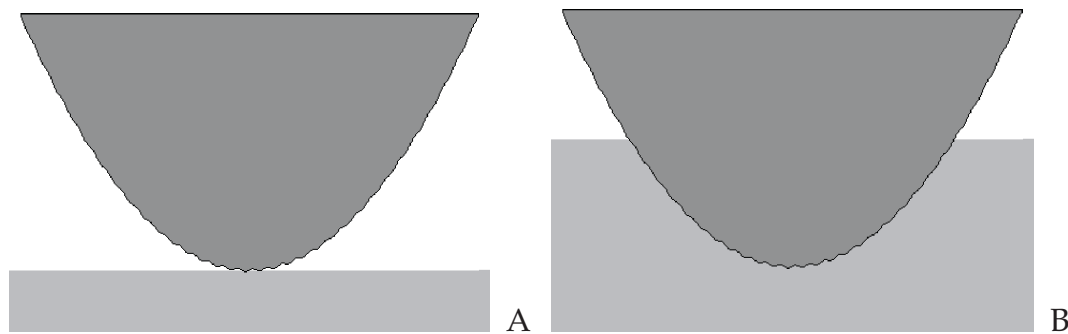


**Figure 2.6:** Definition of a single asperity. A tip with two radii, one large and the other much smaller is indented into a piece of material. A: if the indentation is small, the contact must be considered to consist of several asperities with the smaller radius. B: At larger indentation, the small radius asperities will not significantly affect the strain distribution around the indenter and the tip can be considered a single asperity of the larger radius.

## 2.5 Tips

### Tips for the LFA

One of the features of the LFA is the versatile leafspring unit–tip assembly. Several experiments can be performed using a single leafspring unit and several tips or vice versa. The choice of tips is virtually unlimited. Two kinds of tips have been used with the LFA so far, commercially obtained diamond tips and etched tungsten wire. The first type of tips was used in the experiments in chapters 3 and 4.

### What is a single–asperity tip?

In order to perform single–asperity experiments, a single–asperity tip is needed. Unfortunately, the definition of a single–asperity is somewhat ambiguous. The definition used in this thesis is: *'A single–asperity tip is a tip that can be described with one single radius. Deviations from this single radius do not significantly affect the experimental results compared to a flawless tip'*, see figure 2.6.

This definition might come across as somewhat pragmatic. However, this approach can be supported theoretically. Most relevant in this regard is the paper by Greenwood and Wu [11] which concerns the nature of rough contacts. They argue that the nature of a rough contact is best described using Archard's description [12] which states that the relevant asperity size is not automatically that of the shortest length scale, but rather should be related to a length–scale dependent on the indentation. If a tip with a micron size radius and nanometre scale protrusions is indented more than a few nanometres, the global micrometre scale radius will determine the stress and strain distribution around the contact and the effect of the nanometre size im-

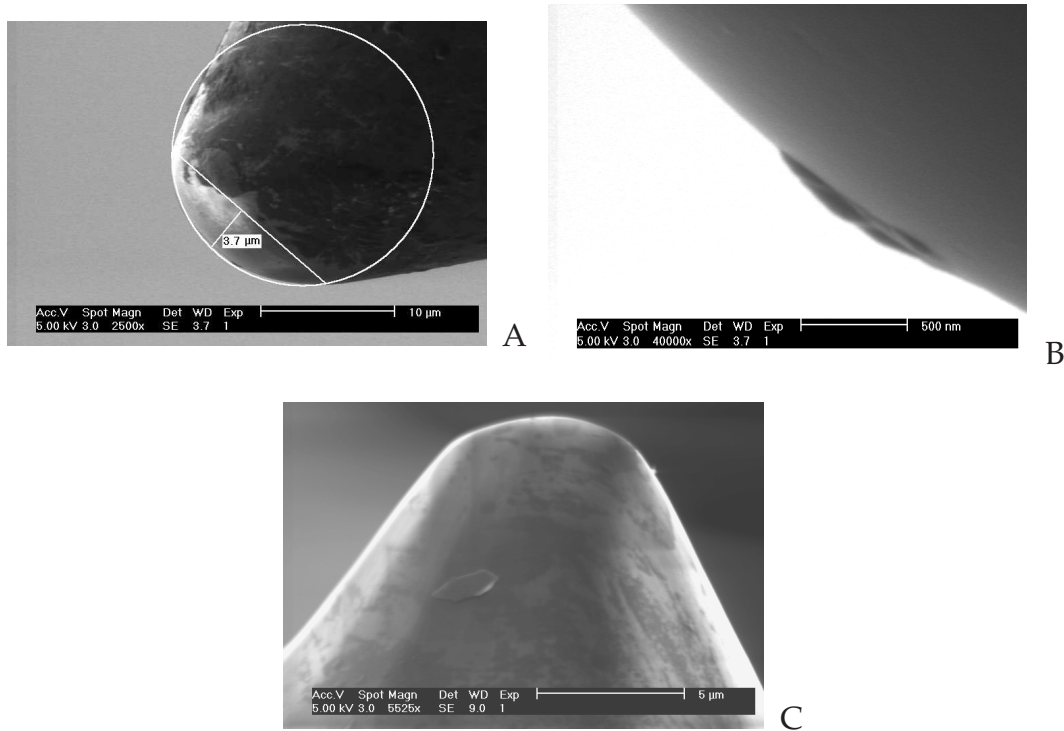


**Figure 2.7:** SEM images of diamond tips. The images of the 10  $\mu\text{m}$  tip (A, B) were made after use in the LFA. The layer of pollution can be removed by scratching the tip bi-directionally across the sample, in this case at an indentation of 3.7  $\mu\text{m}$  (A). 20 nm protrusions were found near the apex of the tip, this is small enough to consider the tip smooth for the experiments in this thesis (B). The image of the 5  $\mu\text{m}$  tip was taken before the experiments described in chapters 3 and 4 were performed with it (C).

perfections will be negligible; the tip can be considered a single asperity. If this tip is used to measure nanometre size indentations, the contact is not a single-asperity contact, but rather a contact of multiple nanometre sized asperities.

## Diamond tips

Diamond tips, polished to radii varying from 0.7 to 50  $\mu\text{m}$ , were obtained from Synton in Lyss, Switzerland. Although not perfectly spherical, these tips showed only minor surface roughness ( $\approx 20$  nm for the 10  $\mu\text{m}$  radius tip). Visual inspection for tip faults was performed using a Scanning Electron Microscope.

One issue that was identified was the pollution of the tips. In figure 2.7 a layer of pollution can be seen at 3.8  $\mu\text{m}$  from the apex. This pollution occurs during tip handling and mounting the tip to the leafspring unit. By first doing a reciprocating run over a stroke of 2 mm at the highest load possible, the tip can be wiped clean. Similar procedures are used in nanoindentation experiments. In some experiments

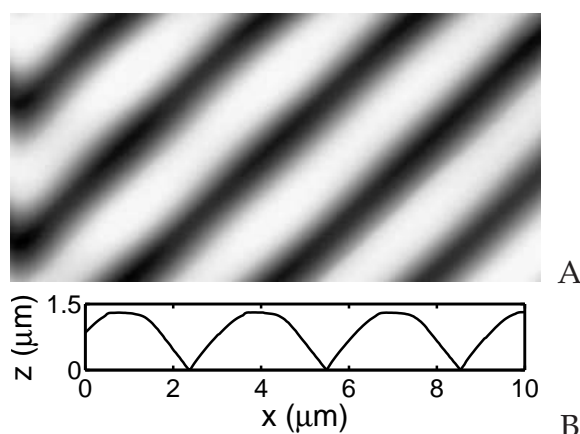


**Figure 2.8:** Embossed surface measured using tapping mode AFM. A 15  $\mu\text{m}$  wide AFM image (A) and profile (B). Each ridge has a radius of approximately 1.5  $\mu\text{m}$ .

the indentation increases in time, see chapter 3, or by repeated motion, see chapter 4. In such cases the experiment with the largest expected indentation was performed repeatedly until reproducible results were obtained.

## Tips obtained by wire etching

Another method of obtaining tips is etching a metal wire. Because of its high modulus of 400 GPa, tungsten is a good choice. The process of etching tungsten wire was originally developed for Scanning Tunnelling Microscopy, STM, where extremely sharp tips are required for optimum resolution [13–15]. This process has been adapted by Hendriks to obtain smooth tungsten tips of larger radius by creating sharp tips using DC potentials and subsequently reducing their radius by switching to AC [10].

Unfortunately tungsten tips prove to be too unstable to allow for prolonged experimentation with a single tip under ambient conditions. Experiments on polystyrene embossed to a pattern of 1.5  $\mu\text{m}$  radius ridges, see figure 2.8, using the same 6  $\mu\text{m}$  radius etched tungsten tip over an interval of several weeks showed the effects of increased tip roughness due to oxidation, see figure 2.9. The geometry of the PS surface causes variation of the contact area and is, as a consequence, extremely sensitive to tip roughness. This is illustrated in figure 2.10. As the tip moves across the ridges, the tip moves up and down along the vertical, or  $z$  axis. This has an immediate effect on the lateral force,  $F_L$ , since the contact area is smaller when the tip is at the apex of a ridge than in the valley between ridges. Where the fresh tip resulted in a smooth  $F_L$  loop as a function of vertical tip position,  $z_{tip}$ , the oxidised tip showed an irregular  $F_L(z_{tip})$  loop. Comparing the tip geometry before and after the experiments, see figure 2.9, shows the full extent of damage the tip has sustained over the one month between both experiments shown in figure 2.10. The first

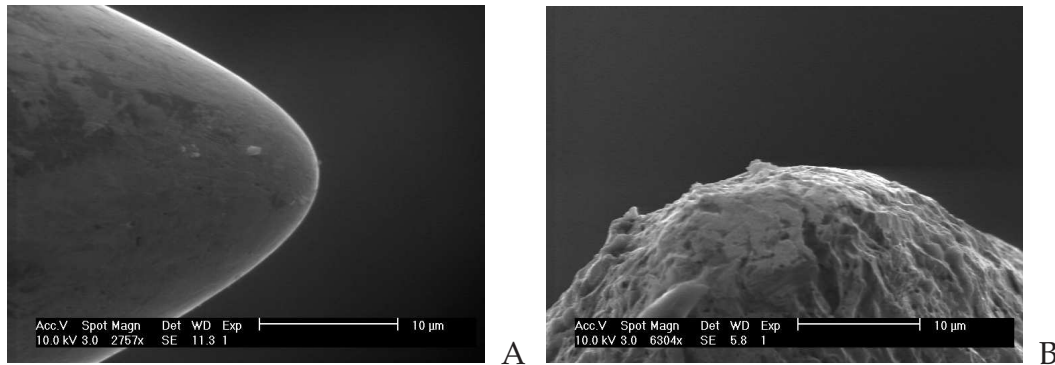


**Figure 2.9:** SEM images of a  $6\ \mu\text{m}$  radius tip etched from tungsten wire shortly after preparation (A) and after one month of experimentation (B). These tips proved to be extremely sensitive to oxidation and could therefore not be used for a prolonged period of time.

symptoms of oxidation were measured after a week. In an attempt to preserve the tungsten tips, they were coated with a cross-linked layer of (tridecafluoro-1,1,2,2-tetrahydrooctyl)trichlorosilane, which would have the added benefit of reducing adhesion. Unfortunately the cross-linking process at  $80\ ^\circ\text{C}$  caused the tip to deteriorate, see figure 2.11.

## Other possibilities for obtaining tips

Besides tungsten and diamond, other obvious tip materials include polished sapphire, glass and silicon, materials with high moduli that are commercially available as tips or spheres. It is also possible to obtain tips by etching or polishing other materials to tips.

## 2.6 Operation

### Leafspring unit preparation

The leafspring units are obtained from an electroplating company, the full process is described in [10]. These leafspring units need to be fitted with a silver coated PET reflective foil in order to be suited for the focus error measurement. This foil is glued to the leafspring unit using paraffin, the tip is fitted into the shaft using the same method. The shaft for mounting the tip connects both normal direction leafsprings, the tip presses against the closed end of the shaft, see figure 2.12. Before fitting the tips, the leafspring unit stiffness is determined in a 2 point bending experiment with a micro-indenter.

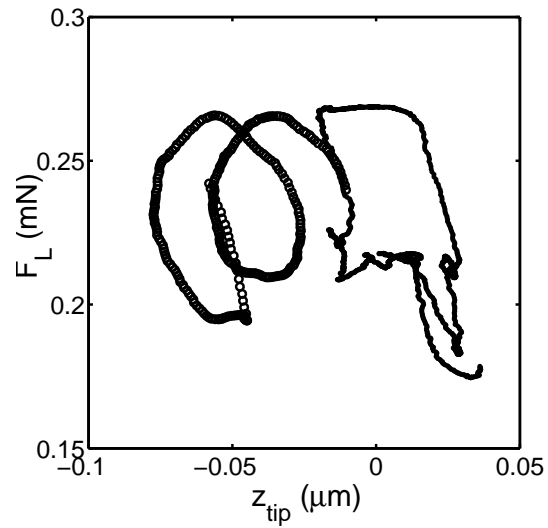


**Figure 2.10:** Relation between lateral force ( $F_L$ ) and vertical displacement ( $z_{tip}$ ) as a  $6 \mu\text{m}$  radius  $W$  tip moves over a  $1.5 \mu\text{m}$  radius ridged PS surface using a fresh tip ( $\circ$ ) and a tip that's been exposed to ambient conditions for a few weeks ( $\cdot$ ).

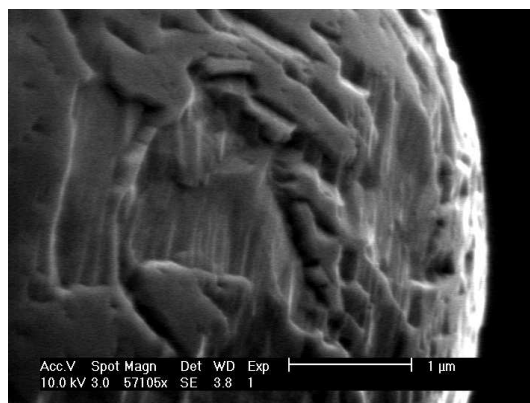


**Figure 2.11:** Tungsten tip after application of a cross-linked (tridecafluoro-1,1,2,2-tetrahydrooctyl)trichlorosilane layer.



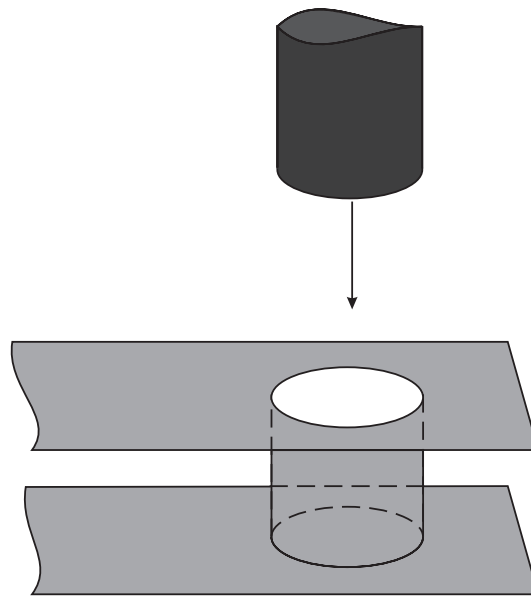


**Figure 2.12:** Schematic representation of the double leafspring/tip assembly. The tip is placed inside the shaft until it rests against the leafspring opposite the open end of the shaft.

## Calibration

The piezo actuator for the  $z$ -motion needs to be re-calibrated each time maintenance has been performed on the force measurement head. This measurement is performed using a dielectric sensor to measure a gap-width as a function of piezo excitation. An aluminium block is placed in the leafspring unit mounting point and its movement with regard to the housing is measured as a function of piezo excitation voltage. The  $z$ -motion in experiments is determined using a linear relation between these two parameters. For calibration of the focus error system, the piezo hysteresis is characterised for a  $22\ \mu\text{m}$  sinusoidal excitation at frequencies of 1 and 0.01 Hz.

After a leafspring unit has been mounted the focus error measurement has to be re-calibrated. This procedure is nearly identical to the one described in [10] with minor adaptations. The Focus Error Signal (FES) in the  $z$  direction is calibrated by pressing the tip onto a silicon wafer using a 0.01 Hz sinusoidal piezo excitation of  $22\ \mu\text{m}$ . This excitation is large enough to characterise the full FES response across the focus error measurement range. Crosstalk from the  $z$  deflection measurement to the  $x$  deflection measurement is subsequently measured by applying a similar excitation at 1 Hz.

The lateral, or  $x$  FES response is calibrated by pushing the leafspring aside across the focus error measurement range using the positioning stage in a manner similar to that described in [10]. Calibration of the crosstalk from the  $x$  to the  $z$  direction FES measurement is also unchanged with regard to [10] and performed by gently brushing the leafspring unit in the lateral direction.

## Experiments

Performing experiments using the LFA is relatively straightforward. However, different types of measurements will result in different sources of errors. It has already been illustrated in section 2.3 that there are several limitations at the lower and upper end of the velocity range, these can be worked around using the right settings.

### Maximising the measurement accuracy

There are a few rules of thumb for minimising the effect of the errors inherent to the device. The first rule is to maximise the sensitivity, the second is to perform dedicated calibrations, the third is to fine-tune the PID settings of the feedback loops.

The sensitivity can be maximised in several manners. The amplification of the driving system signals before A/D conversion can be adjusted to maximise the digital resolution of the measured signal. In low force ranges one option is to use a leaf-spring unit of lower stiffness. This results in more sensitive force measurements, but can also lead to stick-slip [4, 16]. Decreasing the voltage range of the A/D converters allows for more sensitive FES measurements. However, the accuracy of the FES measurement remains limited by optical quality.

The most influential errors inherent to the LFA are the hysteresis and drift of the piezo actuator. Hysteresis can be minimised, and the remaining drift can be characterised, by performing drift measurements on silicon wafers. The hysteresis and drift can be reduced by setting the FES value desired for the normal force and lowering the tip onto the sample until the piezo excitation reaches approximately 20  $\mu\text{m}$ . After about 100s the relation between piezo response to the excitation voltage will be described adequately by a linear relation once sliding begins. This protocol allows for accurate indentation measurement in the experiments described in chapter 4.

In chapter 3 indentation creep experiments of 1000 seconds are dealt with. For these measurements an additional calibration of the piezo response is required. By repeating the same experiments on silicon, the piezo response during the indentation part of the experiment could be quantified and corrected for.

## 2.7 Conclusion

The LFA, Lateral Force Apparatus, is a versatile experimental device for microscopic tribological experimentation. It allows for independent measurement of normal and lateral forces and displacements of any variety of material contacts. Its new positioning system allows for the measurement of friction over five decades of sliding velocities and its accurate positioning measurement allows for experiments where the position of the indenter on the sample is relevant.

## References

- [1] Zijlstra, T., Heimberg, J. A., van der Drift, E., Glastra van Loon, D., Dienwiebel, M., de Groot, L. E. M. and Frenken, J. W. M. (2000). Fabrication of a novel scanning probe device for quantitative nanotribology. *Sens. and Act. A*, **84**, 18–24.
- [2] Kaneko, R., Nonaka, K., and Yasuda, K. (1988). Scanning tunneling microscopy and atomic force microscopy for microtribology. *J. Vac. Sci. Technol. A*, **6**, 291–292.
- [3] Lu, C. J., Jiang, Z. G., Bogy, D. B. and Miyamoto, T. (1995). Development of a new tip assembly for lateral force microscopy and its application to thin-film magnetic media. *J. Tribol-T. ASME*, **117**, 244–249.
- [4] Vellinga, W. P. and Hendriks, C. P. (2001). Sliding friction dynamics of hard single asperities on soft substrates. *Phys. Rev. E*, **63**, 066121–1–066121–14.
- [5] Sills, S. and Overney, R. M. (2003). Creeping friction dynamics and molecular dissipation mechanisms in glassy polymers. *Phys. Rev. Lett.*, **91**, 95501–1–95501–4.
- [6] Dienwiebel, M., Verhoeven, G. S., Pradeep, N., Frenken, J. W. M., Heimberg, J. A. and Zandbergen, H. W. (2004). Superlubricity of graphite. *Phys. Rev. Lett.*, **92**, 126101–126104.
- [7] Johnson, K. L., Kendall, K. and Robbets, A. D. (1971). Surface energy and the contact of elastic solids. *Proc. R. Soc. Lond. A*, **324**, 301–313.
- [8] Baumberger, T. and Caroli, C. (1998). Multicontact solid friction: A macroscopic probe of pinning and dissipation on the mesoscopic scale. *MRS Bull.*, **23**, 41–46.
- [9] Hendriks, C. P. and Vellinga, W. P. (2000). Quantitative measurement of sliding friction dynamics at mesoscopic scales: The lateral force apparatus. *Rev. Sci. Instr.*, **71**, 2391–2402.
- [10] Hendriks, C. P. *Quantitative measurement of friction dynamics at mesoscopic scales: development and performance of the LFA*. PhD thesis, Technische Universiteit Eindhoven, 2000.
- [11] Greenwood, J. A. and Wu, J. J. (2002). Surface roughness and contact: an apology. *Meccanica*, **36**, 617–630.
- [12] Archard, J. F. (1957). Elastic deformation and the laws of friction. *Proc. Roy. Soc. A*, **243**, 190–205.
- [13] Kerfriden, S., Nahlé, A. H., Campbell, S. A., Walsh, F. C. and Smith, J. R. (1998). The electrochemical etching of tungsten STM tips. *Electrochim. Acta*, **43**, 12–13.
- [14] Müller, A.-D., Müller, F., Hietschold, M., Demming, F., Hersh, J. and Dickmann, K. (1999). Characterization of electrochemically etched tungsten tips for scanning tunneling microscopy. *Rev. Sci. Instrum.*, **70**, 3970–3972.
- [15] Guise, O. L., Achner, J. W., Jung, M.-C., Coughnour, P. C., and Yates Jr., J. T. (2002). Reproducible electrochemical etching of tungsten probe tips. *Nano Lett.*, **2**, 191–193.
- [16] Vellinga, W. P. and Henriks, C. P. (2000). Sliding friction dynamics of hard single asperities on soft surfaces. *Tribol. Lett.*, **9**, 119–124.

## CHAPTER THREE

# Velocity dependence of friction on polystyrene (PS)<sup>1</sup>

---

### 3.1 Introduction

#### Friction dynamics

The Amontons–Coulomb law, that relates friction force to normal force through the coefficient of friction, is frequently used. Like the so-called Young’s modulus, a friction coefficient offers designers a handy and simple tool to estimate the performance of a material using one constant. Unfortunately, like with the Young’s modulus, a single coefficient is not always sufficient to predict material performance. This is especially true for contacts involving materials with time dependent properties, such as polymers, but also in other material combinations where friction depends on sliding velocity and other parameters, such as normal force, time and, of course, temperature. With narrow design margins, a single coefficient can be insufficient to describe friction to the desired degree of accuracy.

Also within wide design margins, rate dependent material behaviour can cause problems, for example as a source of frictional vibration. The occurrence of stick–slip [1] has been shown to be caused by growth of the real contact area with contact time due to creep [2]. The contact area is usually proportional to the friction force. However, this proportionality only occurs when the shear stress acting on that contact area can be considered constant and there is a linear relation between the real contact area

---

<sup>1</sup>Parts of this chapter are taken from R. P. Schaake, W. P. Vellinga and H. E. H. Meijer: *Microtribological behaviour of monodisperse polystyrene* In *Transient Processes In Tribology: Proceedings of the 30th Leeds-Lyon Symposium on Tribology* held at INSA de Lyon Villeurbanne, France 2nd-5th September 2003, p.p. 507–517. And from R. P. Schaake, W. P. Vellinga, J. M. J. den Toonder and H. E. H. Meijer: *Quantitative microscopic single-asperity friction measurements on PS*, submitted to *Tribology Letters*

and the normal load. In the sliding of materials with time dependent or non-linear mechanical properties, such as polymers, the Amontons–Coulomb law will be insufficient to explain the frictional behaviour. Growth of the contact area with contact time will lead to a decrease of friction force with increasing sliding velocity, referred to as velocity weakening. The opposite effect, increasing friction force with increasing sliding velocity is referred to as velocity strengthening and must be related to an increase in the shear stress. Both rate effects can be described using creep and relaxation laws in rate–and–state equations [3–6].

In this chapter friction dynamics originating from velocity dependent friction are described using rate–and–state equations combined with steady state friction experiments to study single–asperity friction dynamics arising from the rate–dependent behaviour of polystyrene. It is verified whether friction can be expressed in terms of rate–and–state equations, i.e. that it can indeed be applied to contacts of different geometries using the same function of time and velocity and results are compared to macroscopic multi–asperity results and FFM results obtained on polystyrene.

## Friction on polystyrene

Friction on polystyrene is not of much industrial relevance. Most sliding applications involve semi–crystalline materials or less brittle amorphous polymers, such as PMMA or polycarbonate. However, polystyrene is an interesting model material for scientific purposes, see e.g. [5–8]. Polystyrene has been thoroughly characterised in many fields relevant for tribology. Polystyrene is not only a frequently used model material for polymer physics, e.g. [9], and the study of glassy polymer mechanical behaviour, e.g. [10], but it has also been used in the study of friction dynamics as a model material for tectonic plates, e.g. [11], and FFM studies, e.g. [7].

Work by Heslot *et al.* [8] on macroscopic contacts indicated an activation volume associated with the de–pinning of static contacts of  $1\text{--}2\text{ nm}^3$ . More recently it was deduced from FFM results that, for atactic PS, the specific molecular de–pinning mechanism responsible for velocity strengthening is the activation of hindered frozen relaxation states [7]. Specifically, an activation energy of 29 kJ/mol was found, a value corresponding to the gamma relaxation, i.e. the rotation of the phenyl groups around the C–C bonds in the PS backbone. The issue of linking these results to the macroscopic scale remains important. For example, in [7] it is suggested that, depending on the degree of size and pressure confinement, other relaxation mechanisms might be involved in macroscopic sliding.

All these factors make polystyrene an interesting choice for the study of single–asperity friction dynamics. In this chapter the LFA is used to determine the influence of creep on single–asperity friction of two polystyrenes of significantly different molar mass.

## Rate-and-state approach

For a macroscopic sliding contact it is expected that the friction force  $F_F$  can be described as the product of an effective velocity dependent shear stress,  $\sigma_s(v_s)$ , and the sum of the area of all the micro contacts,  $A_\Sigma$  [12]:

$$F_F = \sigma_s(v_s) A_\Sigma(\theta) \quad (3.1)$$

Here  $v_s$  is the sliding velocity and  $\theta$  is the contact "age" [2,5,6]. In steady sliding, the contact age,  $\theta$ , is related to  $v_s$  via:

$$\theta(v_s) = D/v_s \quad (3.2)$$

where  $D$  is the diameter of the average micro contact, or in a single-asperity contact the contact diameter. Another length-scale is  $L$ , characteristic for the transition from steady sliding to stick-slip, chosen so that stick-slip occurs when:

$$k_L < k_C \quad ; \quad k_C = \partial F_F / \partial L \quad (3.3)$$

with  $k_L$  the lateral stiffness of the loading mechanism and  $k_C$  the lateral contact stiffness. In stick-slip experiments,  $L$  is of the same order of magnitude as  $D$  [3].

The definition of "asperity" and, as a consequence, contact diameter  $D$ , is dependent on the contact conditions. With increasing loads individual contacts will merge [2], to form a single, large, contact. As a consequence, nanometre sized protrusions on micron sized asperities have no significant effect on the stress and strain distribution around micrometre scale indentations, see figure 2.6 [13]. Also, the use of a contact diameter is somewhat misleading in macroscopic contacts since the actual micro-contacts are rarely circular [2]. Using single, spherical, asperities will allow for a more accurate study of the relation between  $L$  and the contact diameter  $D$ , a single contact with contact area  $A_c$  can be created and studied as a function of contact age, normal force and tip radius.

The contact area  $A_c$  is a function of the contact age  $\theta$  and as such depends on the sliding velocity, see equation 3.2. In the case of single-asperity measurements,  $A_c(\theta)$  can be considered equal to the apparent area of contact. To translate equation 3.1 to a rate-and-state description of a microscopic single-asperity contact between a hard tip and a compliant material, e.g. a polymer, the contact area can be described as an elastic Hertzian contact area  $A_{c0}$  for contacts between a single rigid asperity with radius  $R$  and a flat surface with a reduced elastic modulus  $E^* = E/(1 - \nu)$ , where  $\nu$  is the Poisson ratio:

$$A_{c0} = \pi \left( \frac{3F_N R}{4E^*} \right)^{2/3} \quad (3.4)$$

This equation can be extended to incorporate creep in a manner analogous to one commonly applied in the rate-and-state description of multi-asperity contacts [6]:

$$A_c(\theta) = A_{c0} \left[ 1 + m \ln \left( 1 + \frac{\theta}{\theta_0} \right) \right] \quad (3.5)$$

at contact times  $\theta > \theta_0$  the contact grows due to creep, leading to velocity weakening,  $\theta_0$  is the time required for creep to initiate.

Velocity strengthening effects do not originate from  $A_c(\theta)$ , but can be described in the form of a rate dependent shear stress,  $\sigma_s(\dot{\epsilon}_s)$ , where the shear rate  $\dot{\epsilon}_s = v_s/h$  with  $h$  the thickness of the sheared layer [14]. The shear stress  $\sigma_s(\dot{\epsilon}_s)$ :

$$\sigma_s(\dot{\epsilon}_s) = \sigma_{s0} \left[ 1 + \alpha \ln \left( 1 + \frac{\dot{\epsilon}_s}{\dot{\epsilon}_{s0}} \right) \right] \quad (3.6)$$

Where  $\sigma_{s0}$  is the shear stress at low shear rates and  $\dot{\epsilon}_{s0}$  is the shear rate above which the shear stress is rate dependent. In the following it is assumed that  $h$  is constant, therefore  $\dot{\epsilon}_s \propto v_s$ . Subsequently  $\dot{\epsilon}_s$  is substituted with  $v_s$  and  $\dot{\epsilon}_{s0}$ , with the corresponding sliding velocity  $v_{s0}$ . The dimensionless constants  $\alpha$  and  $m$  determine the respective slopes;  $m$  describes the creep rate and  $\alpha$  describes the increase in shear stress with sliding velocity [5,6]. The latter can be expressed as the ratio between the atomic kinetic energy and a material-specific activation energy [6]:

$$\alpha = \frac{k_B T}{\sigma_{s0} V_{act}} \quad (3.7)$$

where  $k_B$  is Boltzmann's constant,  $T$  the temperature, and  $V_{act}$  the activation volume of the relevant local dynamical process [14]. The product of equations 3.5 and 3.6 gives the following relation equivalent to 3.1:

$$F_F = \sigma_{s0} A_{c0} \left[ 1 + \alpha \ln \left( 1 + \frac{v_s}{v_{s0}} \right) \right] \left[ 1 + m \ln \left( 1 + \frac{\theta}{\theta_0} \right) \right] \quad (3.8)$$

which will be used to analyse the data.

In this approach stationary and sliding contacts are considered to be equivalent. In both cases the contact area grows in time, the largest difference being that in stationary contacts  $v_s = 0$  nm/s. It is generally assumed that upon incipient sliding  $v_s \ll v_{s0}$  and  $\sigma_s \approx \sigma_{s0}$  [6], implying that the friction upon incipient sliding can be described as a function of the contact area only.

## Slide–hold–slide experiments

In macroscopic experiments rate-and-state laws combined with slide–hold–slide experiments [4, 11] have proven to be an effective method for understanding the role

of time-dependent material behaviour in friction. This combination is so effective because it allows for steady-state measurements of the relevant parameters which can later be used to describe dynamic friction.

In slide–hold–slide experiments a reproducible contact situation is created by sliding over a distance long enough to achieve steady sliding conditions at a refresh velocity,  $v_{sr}$ . The motion is then halted for a hold time  $t_h$ . After  $t_h$  the motion is resumed and  $F_{Fmax}(t_h)$  is measured followed by  $F_F(v_s)$ .

In this chapter results obtained using a single–asperity variant of the slide–hold–slide protocol are discussed. In addition to forces, sliding velocities and waiting time, the contact time and contact area were measured.

## 3.2 Materials and method

### Materials

Polystyrenes of two different molar masses were used: a low (PS 56),  $M_N = 56$  kg/mol,  $M_W/M_N = 1.05$ , and a high a high molar mass (PS 1000),  $M_N = 966$  kg/mol,  $M_W/M_N = 1.15$ . The materials, supplied by John Gearing Scientific, were first pressed into 0.5 mm thick plates at 180°C for 10 minutes under a load of 300 kN and subsequently cooled to ambient temperature, and pressed under a load of 100 kN. Samples were cut from these plates and subsequently embossed with a silicon wafer at 110-120 °C, depending on the viscosity of the sample, to obtain a smooth surface. The silicon wafer was coated with cross-linked (tridecafluoro-1,1,2,2-tetrahydrooctyl)trichlorosilane to ease release, without polluting the sample surface. The thickness of the samples decreased slightly during this step so the final sample thickness was  $0.4 \pm 0.1$  mm. These samples were subsequently stored at ambient conditions for at least a week.

### Slide–indent–slide experiments

Slide–indent–slide experiments were performed, see figure 3.1. After applying the normal load,  $F_N$ , a reproducible starting situation was created sliding the tip at a certain refresh velocity,  $v_{sr}$ , in steady sliding. The motion was then halted for a hold time,  $t_h$ , after which it was resumed at sliding velocity  $v_s$ . These slide–indent–slide experiments differ from the macroscopic slide–hold–slide experiments in that they are performed using a single asperity contact and that the contact area is unambiguous and can be quantified. The contact area is estimated from the track left after the experiment. From FEM modelling of indentation experiments it is known that, for the loading conditions used, only a small plastic zone exists at the edge of the contact [15, 16]. Upon unloading the location of this plastic zone will be underneath the summit of the pile-up of the contact. It is assumed that this is not only valid for



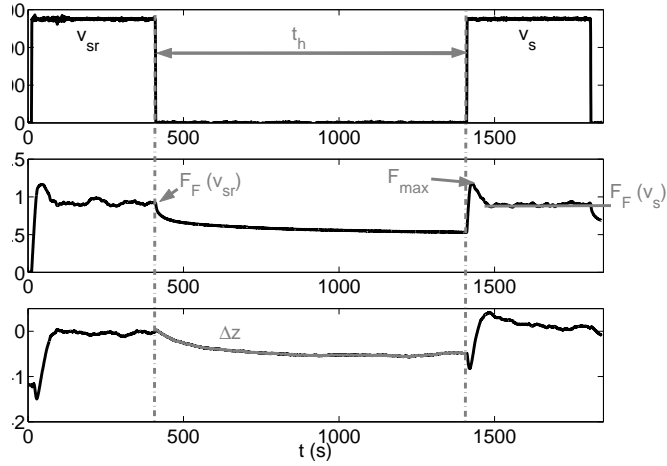


**Figure 3.1:** The slide-indent-slide protocol. From top to bottom, stage velocity  $v_{stage}$ , friction force  $F_F$  and indentation  $z$ .

indentation, but also in sliding.

During  $t_h$  the increase in indentation depth  $\Delta z(t_h)$  is measured to quantify the changes in the contact area. At small indentations, as is the case in these experiments, the relation between contact diameter,  $D$ , and indentation,  $z$ , is  $D = \sqrt{8zR}$ , with  $R$  being the tip radius. This way both  $F_{Fmax}$  and  $F_F$  can be quantitatively related to the contact area.

### Experimental conditions

A diamond tip with  $R = 10\mu\text{m}$  was mounted onto a cantilever unit of normal stiffness  $k_N = 1.72\text{ kN/m}$ , lateral stiffness  $k_L = 540\text{ N/m}$  with a cross talk between the normal and lateral force measurement of 5% and vice versa. Experiments with this tip/cantilever combination were performed at  $F_N = 10\text{ mN}$ . A second diamond tip with  $R = 5\mu\text{m}$ , was mounted onto a different cantilever unit with  $k_N = 0.24\text{ kN/m}$  and  $k_L = 54\text{ N/m}$  with a maximum cross talk of 2.5%. This second cantilever/tip combination was only used for measuring  $F_F(v_s)$  at normal loads of  $F_N = 1\text{ mN}$  and  $2.5\text{ mN}$ .

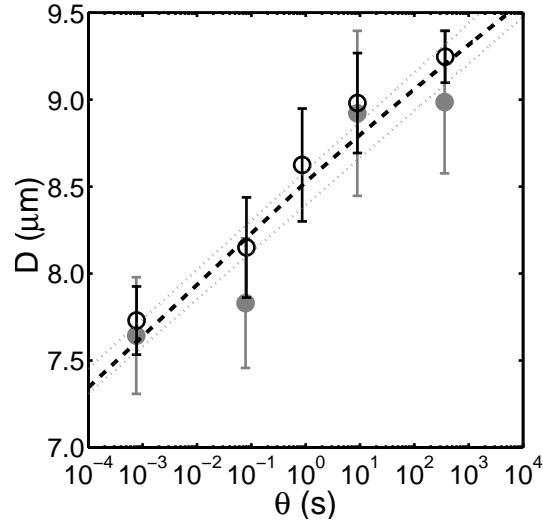


**Figure 3.2:** Contact diameter  $D$  as a function of contact age  $\theta$  for PS 56 ( $\bullet$ ) and PS 1000 ( $\circ$ ). A proportional relation between  $\ln(\theta)$  and  $D^2$  was found (- -). Fits to the individual data sets ( $\cdot\cdot$ ) are clearly not significantly different when compared to the measurement's error

## 3.3 Results and discussion

### Dynamic friction

#### Contact area

Figure 3.2 shows the contact diameter  $D$  of the scratches made with the  $R = 10\mu\text{m}$  tips determined as explained in section 3.2 for different contact ages,  $\theta$ , on PS 56 and PS 1000. No region was detected where  $D$  was independent of  $\theta$  within the measurement range. Therefore  $\theta_0$  and  $A_{c0}$  could not directly be determined but they must be smaller than  $10^{-3}$  s and  $56\mu\text{m}^2$ , respectively. A value of  $A_{c0} = 10.7\mu\text{m}^2$  at very low  $\theta$  (representative for a Hertzian contact situation using  $E = 3$  GPa and  $\nu = 0.33$ ) was taken. Using this value equation 3.5 was fitted to the data, as shown in figure 3.2. The best fits to both data sets were not significantly different and a value of  $m = 2.5$  was found, independent of molar mass.

#### Friction

Figure 3.3 shows the dynamic friction force  $F_F$  as a function of contact age  $\theta$  measured in slide-indent-slide experiments. A best fit of equation 3.8 to the experimental values of  $F_F$  for  $R = 10\mu\text{m}$ , and  $F_N = 10$  mN (circles) was determined for both materials. PS56 showed velocity weakening behaviour throughout the velocity range that spans approximately 5 decades, for two different experimental conditions

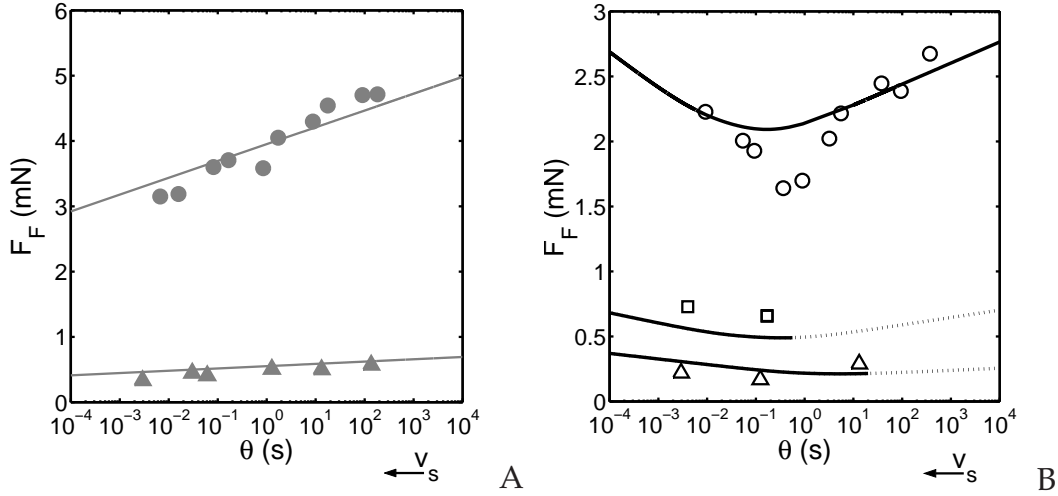


**Figure 3.3:**  $F_F$  as a function of contact age  $\theta$ . The lines are predictions using best fit parameters to the data for  $F_N = 10$  mN,  $R = 10 \mu\text{m}$ . A: For PS56.  $F_N = 10$  mN,  $R = 10 \mu\text{m}$  ( $\bullet$ ) and for  $F_N = 1$  mN,  $R = 5 \mu\text{m}$  ( $\blacktriangle$ ). B: For PS 1000. data for  $F_N = 10$  mN;  $R = 10 \mu\text{m}$  ( $\circ$ ),  $F_N = 2.5$  mN;  $R = 5 \mu\text{m}$  ( $\square$ ) and  $F_N = 1$  mN;  $R = 5 \mu\text{m}$  ( $\triangle$ ). The dotted lines indicate stick-slip occurred in the experiments.

$R = 10 \mu\text{m}$  and  $F_N = 10$  mN, and  $R = 5 \mu\text{m}$  and  $F_N = 1$  mN. Since no velocity strengthening was measured the parameters  $v_{s0}$  and  $\alpha$  could not be determined for PS56. For the low molar mass PS56, it was found that  $\sigma_{s0} = 69$  MPa.

In contrast to the results on low molar mass PS, the friction force measured on high molar mass PS shows a transition from velocity weakening at low velocities, or high  $\theta$ , to velocity strengthening around  $v_s = 10 \mu\text{m/s}$ , or  $\theta \approx 1$  s. From the best fit with equation 3.6 the following values were determined  $\sigma_{s0} = 38$  MPa,  $v_{s0} = 9 \mu\text{m/s}$  and  $\alpha = 0.09$ . Using these parameters in equation 3.8, a good prediction of experimental results measured with a tip of  $R = 5 \mu\text{m}$  under different normal loads was found, see figure 3.3.

Experimental values for  $\sigma_s$  were determined by dividing  $F_F(\theta)$  by  $A_c(\theta)$ . Figure 3.4, shows the values of  $\sigma_s(v_s)$  as well as a best fit using equation 3.6. A good match is found and, interestingly, at sliding velocities of  $v_s \approx v_{s0}$  the shear stress,  $\sigma_s$ , becomes slightly less than  $\sigma_{s0}$  for PS 1000.

## Static contacts

For the quantification of creep during  $t_h$ , equation 3.5 can be used. Because the contact state in rest is not necessarily the same as in sliding,  $\theta_0$  is substituted with an equivalent characteristic time  $\tau$ .

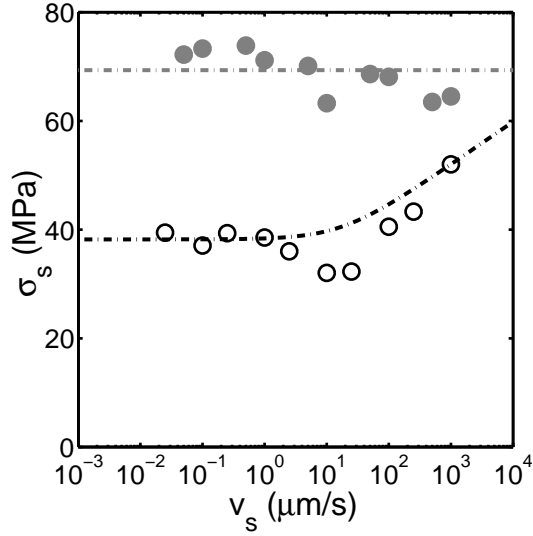


**Figure 3.4:** Shear stress,  $\sigma_s = F_F/A_c$ , in the contact area measured on PS 1000 ( $\circ$ ) and PS 56 ( $\bullet$ ). The lines show the best fit with equation 3.6, the symbols are the measured data for  $F_N = 10$  mN;  $R = 10\mu\text{m}$ .

$$A_c(\theta_r, t_h) = A_c(\theta_r) \left[ 1 + m_c \ln \left( 1 + \frac{t_h}{\tau} \right) \right] \quad (3.9)$$

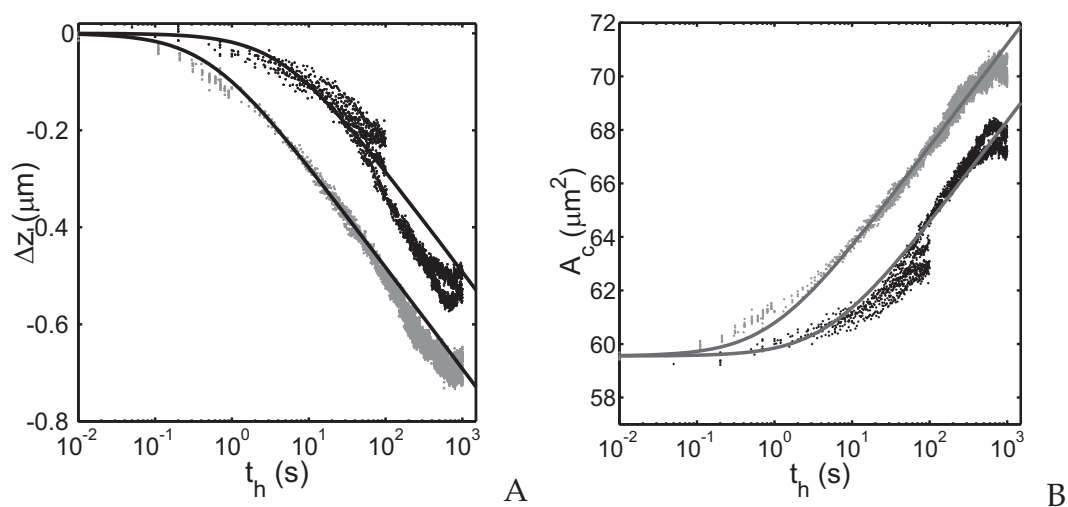
Where  $\theta_r$  is the contact age during steady sliding at refresh velocity  $v_{sr}$ , and  $m_c$  is a dimensionless parameter that describes the creep rate, similar to  $m$  in equation 3.5.

Figure 3.5 shows the creep curves of both PS grades at  $v_{sr} = 2.5\mu\text{m/s}$ . While no significant difference in contact area was found during sliding, a clear effect of molar mass on the indentation was found while the motion was held. When fitting the creep data with equation 3.9, a value of  $m_c = -0.05$  was found for both molar masses, while  $\tau$  was larger for PS 1000 ( $\tau = 5$  s) than for PS 56 ( $\tau = 0.9$  s).

### Peak Friction

From the growth of the contact area  $A_c$  with  $t_h$ , an increase of  $F_{max}$  is expected. There is indeed a slight increase of  $F_{Fmax}$  with  $t_h$ , see figure 3.6. According to the assumptions of the rate-and-state equations, the shear stress at  $\sigma_{smax}$  at  $F_{Fmax}$  should be  $\sigma_{s0}$ , independent of the contact history since  $\dot{\epsilon}_s \ll \dot{\epsilon}_{s0}$ , see section 3.1. However, when calculating  $F_{Fmax}$  using  $\sigma_s = \sigma_{s0}$ , with  $\sigma_{s0}$  derived from steady sliding, and the measured values of  $A_c(\theta_r, t_h)$ , a poor prediction of the measured values is found, see figure 3.6. Apparently the friction upon incipient sliding is not so similar to steady sliding that the same shear stress,  $\sigma_{s0}$ , can be used to describe it.

During hold, there is a significant relaxation of the shear stress,  $\sigma_s$ , acting on the con-



**Figure 3.5:** Creep curves of PS 56 and PS 1000 at  $v_{sr} = 2.5\mu\text{m/s}$  measured with  $R = 10\mu\text{m}$  and  $F_N = 10\text{mN}$ . A:  $\Delta z(t_h)$ . B:  $A_c(t_h)$

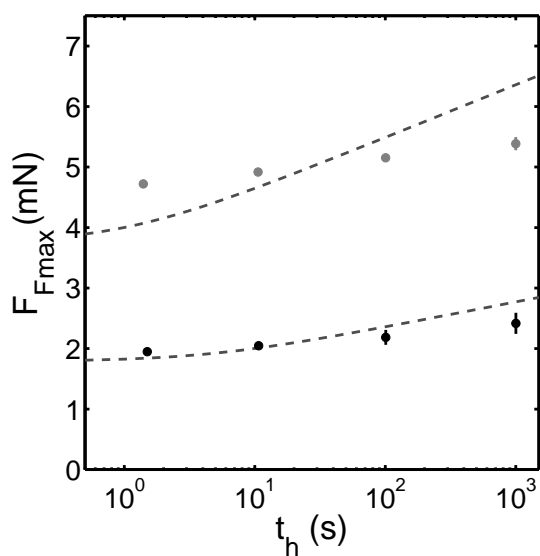


**Figure 3.6:**  $F_{Fmax}(t_h)$  for PS 56 and PS 1000. The points are averages of 3 experiments. The error bars indicate the standard deviation. The dashed lines are predictions with equation 3.8 using the product of an average shear stress  $\sigma_s$  and  $A_c(t_h)$ .

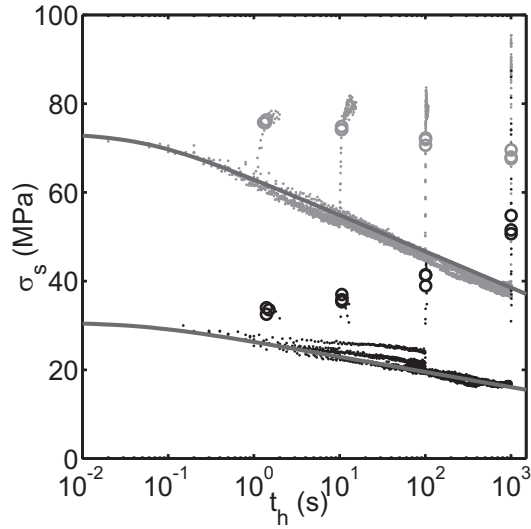


**Figure 3.7:** Shear stress relaxation between  $t_h = 0$  and steady sliding for PS 56 and PS 1000. The lines indicate the fits with equation 3.10, the circles indicate  $\sigma_s$  at  $F_{Fmax}$ . The shear stress continues to rise after  $F_{Fmax}$  has been reached and eventually levels off to the steady state value at  $v_s$ .

tact area. The total decrease in  $F_F$ , while the contact is stationary, is negligible, only  $0.75 \mu\text{N}$ . The relaxation is nearly entirely attributable to an increase of contact area through creep, not to lateral force decay. This relaxation process can be described using the following modified expression of equation 3.6:

$$\sigma_s(t_h) = \sigma_s(v_{sr}) \left[ 1 - \alpha_c \ln \left( 1 + \frac{t_h}{\tau_c} \right) \right] \quad (3.10)$$

Where  $\alpha_c$  is a dimensionless parameter that describes the creep facilitated relaxation rate analogous to  $\alpha$  in equation 3.6 and  $\tau_c$  is a characteristic relaxation time for creep.

The results of the best fit with this equation are also shown in figure 3.7 and reveal that the parameters  $\alpha_c$  and  $\tau_c$  are 0.06 and 0.05 s respectively, independent of molar mass. The only difference in relaxation between both molar mass materials is therefore the shear stress at the refresh velocity  $\sigma_s(v_{sr})$ , ergo the indentation creep is driven by identical lateral relaxation processes.

When motion is resumed, the shear stress increases to a level that increases with  $t_h$ . Just The peak in shear stress occurs after  $F_{Fmax}$  occurs. The maximum shear stress,  $\sigma_{max}$  increases with  $t_h$ .

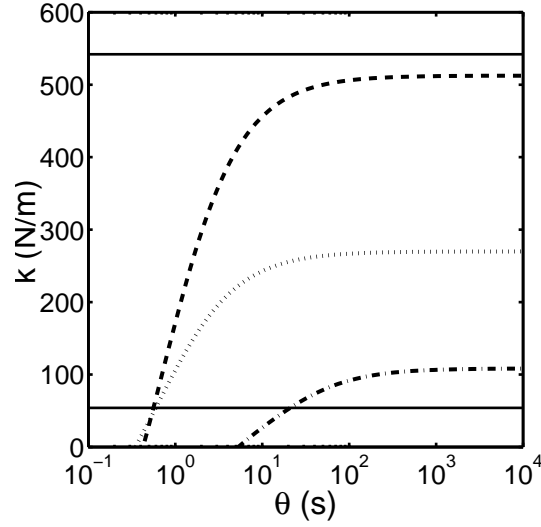


**Figure 3.8:** : Stick–slip estimation, stiffness,  $k$ , as a function of  $\theta$ . The horizontal lines indicate the cantilever stiffness  $k_L$  of the stiff ( $k_L=540$  N/m) and the less stiff ( $k_L=54$  N/m) cantilevers. The contact stiffness  $k_C = \delta F_F / \delta L$  under the various experimental conditions is also given: (- -)  $R = 10\mu\text{m}$ ,  $F_N = 10\text{mN}$ ; ( $\cdot\cdot\cdot$ )  $R = 5\mu\text{m}$ ,  $F_N = 2.5\text{mN}$ ; (- $\cdot$ -)  $R = 5\mu\text{m}$ ,  $F_N = 1\text{mN}$ . If  $k_L > k_C$ , no stick–slip occurs, if  $k_L < k_C$  stick–slip does occur. The best prediction of stick–slip occurring in measurements with the  $R = 5\mu\text{m}$  tip was found for  $L = 1.5 - 2D$ .

## Discussion

The results clearly show that both static and sliding contacts can be described and studied well using equivalent sets of rate–and–state equations. However, although there is some analogy between static and dynamic friction as a function of contact time, the parameters are quantitatively different.

The rate–and–state approach was originally developed as a tool to predict stick–slip [1]. In figure 3.8 the contact stiffness is compared to the lateral stiffness of the cantilevers used, see equations 3.2 and 3.3. It was found that the characteristic length scale  $L$  should be between 1.5 and  $2D$  in order to accurately predict the occurrence of stick–slip in our experiments. While  $L$  and  $D$  cannot be discerned in macroscopic multi–asperity contacts, they can be discerned in single–asperity slide–indent–slide experiments.

The growth of sliding contacts  $A_c(\theta)$  is not the same as the growth of stationary contacts  $A_c(t_h)$ . While  $A_c(\theta)$  is independent of molar mass,  $A_c(t_h)$  does appear to be molar mass dependent, compare figures 3.2 and 3.5. Apparently creep is the primary relaxation mechanism for residual shear stress from sliding during hold. Since the shear stress relaxation could be predicted using parameters independent of molar mass, it is assumed that in slide–indent–slide experiments the creep rate depends solely on the relaxation of the residual shear stress in the contact.

FFM experiments, such as performed by Sills and Overney [7] and Kajiyama *et al.* [17], probe volumes within several nanometres of the surface, where molar mass effects on mechanical behaviour are expected, e.g. [18,19]. In such experiments velocity strengthening is observed which can be quantitatively attributed to the kinetics of specific segmental motions [7]. It has been suggested that lower molar mass polymers exhibit a larger chain mobility at the surface [17,18], having a profound effect on the potential energy landscape of the surface. Energy barrier heights between different conformations would decrease, reducing the activation energy for conformation changes. Reductions in molar mass affect the shear stress in a manner similar to a rise in temperature. An increase in temperature would lead to an increase in shear stress [7], the increased mobility of molar mass chains is therefore expected to have a similar effect. From equation 3.7 it can be deduced that  $\sigma_{s0} = E_a/V_{act}$ . Fitting the measured data using equations 3.7 and 3.8 an activation energy of the relevant physical processes of  $E_a = 28$  kJ/mol is found, which is very close to the 29 kJ/mol characteristic of the  $\gamma$  relaxation, or phenyl group rotation [20]. Since both materials have a number average molar mass high enough to ascertain 3 entanglements per chain ( $M_e \approx 17.5$  kg/mol [21]), little influence of molar mass on bulk properties is to be expected. Indeed, modulated DSC, or M-DSC, measurements indicated a difference in the bulk  $T_g$  of less than 1K. Since the effect of molar mass on friction is measured as an effect on shear stress which quantitatively corresponds to a specific relaxation mechanism at the surface, it is likely that shear stress in polystyrene friction is indeed determined by surface properties, as postulated by Baumberger *et al.* [5].

If the same relaxation mechanism is the source of the increased shear stress in the LFA experiments described here,  $V_{act}$  has to be  $1.28$  nm<sup>3</sup>. The higher shear stress,  $\sigma_{s0}$ , measured on PS 56 can be explained in two ways. One possible explanation is that the  $\gamma$  relaxation is still the only dissipative mechanism, which would mean the explanation is a temperature shift, or  $T_g$  reduction. Another possibility is that other dissipative mechanisms are responsible for the increase in shear stress. Unfortunately it was not possible to measure the coefficient  $\alpha$  on PS 56 using the current experimental possibilities of the LFA. To achieve this experiments at sliding velocities several orders of magnitude higher than 1 mm/s, or at elevated temperature, would be required.

## Conclusion

**Measurement method.** The combination of a rate-and-state approach with microscopic single-asperity slide-hold-slide experiments has proven to be an effective tool for studying the contribution of different factors to friction. The unequivocal nature of the experiments allows for a quantitative approach which provides relevant insight into the nature of macroscopic contacts, by linking macroscopic and nanoscopic results. Both the dynamic friction force and the occurrence of stick-slip could be predicted for different normal loads and tip radii, using the results obtained



with a different normal load and tip radius. The results are qualitatively in agreement with macroscopic observations from literature [5, 6] and in addition allow for quantification of the mechanisms responsible for velocity weakening, i.e. contact growth, and for velocity strengthening, i.e. the dissipative mechanism. Most importantly the onset of contact growth at longer contact times and shear stress increase at higher sliding velocities can be distinguished from one another, which is not possible in multi-asperity contacts due to the population of contact sizes in such contacts, whereas the single-asperity contact has a defined contact geometry.

**Molar mass effects.** Both the different friction forces measured on both molar masses, and the difference in creep during hold, can be attributed to differences in shear stress response at the surface. Using microscopic single-asperity experiments it was found that molar mass influences the shear stress. Since the molar masses of the materials used are such that molar mass does not significantly influence bulk properties, it can be concluded that shear occurs in a layer close to the surface. The primary relaxation mechanism responsible for the shear stress behaviour measured on the high molar mass material corresponds energetically to the  $\gamma$  relaxation, or phenyl group rotation.

**Static vs. dynamic friction.** Interestingly no difference in contact area was observed between both molar masses during steady sliding, while during hold after sliding relaxation of the shear stress has a pronounced influence on contact growth. On this scale, indentation appears to be more related to bulk properties than to surface properties. However, as relaxation of the shear stress plays a dominant role in contact creep during hold, the molar mass indirectly has a pronounced effect on creep in static shear loaded contacts.

## References

- [1] Dieterich, J. H. (1978). Time-dependent friction and the mechanics of stick-slip. *PAGEOPH*, **116**, 790–806.
- [2] Dieterich, J. H. and Kilgore, B. D. (1994). Direct observation of frictional contacts: New insights for state-dependent properties. *PAGEOPH*, **143**, 283–302.
- [3] Ruina, A. (1983). Slip instability and state variable friction laws. *J. Geophys. Res.*, **88**, 10359–10470.
- [4] Dieterich, J. H. (1979). Modeling of rock friction 1. experimental results and constitutive equations. *J. Geophys. Res.*, **84**, 2161–2168.
- [5] Baumberger, T., Berthoud, P. and Caroli, C. (1999). Physical analysis of the state- and rate-dependent friction law. ii. dynamic friction. *Phys. Rev. B*, **60**, 3928–3939.
- [6] Berthoud, P., Baumberger, T., G'Sell, C. and Hiver, J. M. (1999). Physical analysis of the state- and rate-dependent friction law: Static friction. *Phys. Rev. B*, **59**, 14313–14327.
- [7] Sills, S. and Overney, R. M. (2003). Creeping friction dynamics and molecular dissipation mechanisms in glassy polymers. *Phys. Rev. Lett.*, **91**, 95501–1–95501–4.
- [8] Heslot, F., Baumberger, T., Perrin, B., Caroli, B. and Caroli, C. (1994). Creep, stick-slip, and dry-friction dynamics: experiments and a heuristic model. *Phys. Rev. E*, **49**, 4973–4988.
- [9] Fox, T. G. and Flory, P. J. (1950). Second-order transition temperatures and related properties of polystyrene. i. influence of molecular weight. *J. Appl. Phys.*, **21**, 581–590.
- [10] van Melick, H. G. H., Govaert, L. E. and Meijer, H. E. H. (2003). Localisation phenomena in glassy polymers: influence of thermal and mechanical history. *Polymer*, **44**, 3579–3591.
- [11] Baumberger, T. and Caroli, C. (1998). Multicontact solid friction: A macroscopic probe of pinning and dissipation on the mesoscopic scale. *MRS Bull.*, **23**, 41–46.
- [12] Bowden, F. P. and Tabor, D. (1964). *The friction and lubrication of solids; Part II*. Clarendon Press, Oxford, United Kingdom, 2nd edition.
- [13] Archard, J. F. (1957). Elastic deformation and the laws of friction. *Proc. Roy. Soc. A*, **243**, 190–205.
- [14] Briscoe, B. J. and Evans, D. C. B. (1982). The shear properties of langmuir-blodgett layers. *P. Roy. Soc. Lond. A Mat.*, **380**, 389–407.
- [15] van Melick, H. G. H., Bressers, O. F. J. T. and den Toonder, J. M. J., Govaert, L. E., Meijer, H. E. H. (2003). A micro-indentation method for probing the craze-initiation stress in glassy polymers. *Polymer*, **44**, 2481–2491.
- [16] van Melick, H., van Dijken, A., den Toonder, J., Govaert, L. and Meijer, H. (2002). Near-surface mechanical properties of polymers. *Phil. Mag. A*, **82**, 2093–2102.
- [17] Kajiyama, T., Kawaguchi, D., Sakai, A., Satomi, N., Tanaka, K. and Takahara, A. (2000). Determination factors on surface glass transition temperatures of polymeric solids. *High Perform. Polym.*, **12**, 587–597.

- [18] Jain, T. S. and de Pablo, J. J. (2002). Monte carlo simulation of free-standing polymer films near the glass transition temperature. *Macromolecules*, **35**, 2167–2176.
- [19] Jones, R. A. L. (1999). The dynamics of thin polymer films. *Current opinion in colloid and interface science*, **4**, 153–158.
- [20] Reich, S. and Eisenberg, A. (1972). Theoretical approach to the assignment of molecular mechanisms for cryogenic loss peaks in polymers. *J. Polym. Sci. A-2*, **10**, 1397–1400.
- [21] Aharoni, S. M. (1986). Correlations between chain parameters and the plateau modulus of polymers. *Macromolecules*, **19**, 426–434.

# Molecular weight dependence of polyethylene (PE) wear<sup>1</sup>

---

## 4.1 Introduction

### PE in tribological contacts

Polyethylene (PE), especially High Density PE (HDPE), is a frequently used sliding material [1]. In dry sliding contacts it exhibits low friction and stable sliding behaviour, which is generally attributed to the intrinsic properties of PE. Melt processed PE has a Young's modulus of up to 1.5 GPa, while an oriented single PE chain has a Young's modulus two orders of magnitude higher. Thus individual PE chains are stiff and strong, considering their small diameter, but the interaction between the chains is weak. For ultimate mechanical properties long sections of chains oriented in an extended crystalline structure are required. An example thereof is the Dyneema fibre in which Ultra High Molecular Weight PE (UHMWPE) chains are fully stretched and aligned alongside one another [2], resulting in strong fibres, with a breaking stress of approximately 3 GPa, and stiff, with a Young's modulus of approximately 150 GPa. The weak Van der Waals interactions act along large portions of a chain with neighbouring chains, resulting in efficient transfer of forces from chain to chain at short time-scales [2]. Under prolonged tensile loading the chains will slip alongside one another resulting in creep.

The low friction force is generally attributed to this easy shearing along the chain

---

<sup>1</sup>Parts of this chapter are taken from R. P. Schaake, J. M. J. den Toonder, W. P. Vellinga and H. E. H. Meijer: *One Minute Wear Rate Measurement* In *Transient Processes In Macromolecular Rapid Communications*, Vol. 26 (2005) p.p. 188–191. And from R. P. Schaake, W. P. Vellinga, J. M. J. den Toonder and H. E. H. Meijer: *Quantitative microscopic study of fatigue-type wear on PE*, in preparation

direction in an oriented shear layer, a phenomenon observed in the sliding of HDPE, UHMWPE, and PTFE [3]. This layer is formed by the transfer of polymer to the, usually metal, counter-surface it is sliding against. Forming a smooth oriented polymer layer in the case of HDPE, UHMWPE and PTFE. If this layer is not formed, e.g. when sliding at high sliding velocities, or in polymers that don't show this shearing behaviour, the friction level is higher [4]. In general, the structure of PE sliding parts is not one of perfectly aligned chains, but consists of folded chain crystals separated by amorphous regions. Therefore, the shearing of inter-chain interactions is still easy since it occurs at a local microscopic length-scale, rather than occurring throughout the the material as in the strain loading of a Dyneema fibre.

The downside is that every easy shearing mechanism goes hand in hand with a low wear resistance. Therefore, high molar masses are required to improve wear resistance, since longer chains have more interaction with surrounding chains [5]. This generally means that in sliding applications where wear resistance is critical UHMWPE is used rather than HDPE. The disadvantage of UHMWPE compared to HDPE is that it cannot be melt processed, e.g. via extrusion or injection moulding, since its viscosity and melt elasticity are too high. The combined friction and wear performance of UHMWPE have made it a common material for friction surfaces, despite these obvious processing disadvantages.

## **Wear of polyethylene**

Wear of PE occurs through three major wear mechanisms: abrasive, fatigue and adhesive wear [6]. In abrasive wear material is removed by cutting or ploughing at an asperity level. In fatigue wear material is removed after having locally failed by repeated straining near the surface. Adhesive wear occurs when a transfer layer is formed. This layer protects the PE surface from a direct cutting action and acts as an intermediate stage in the wear process; material adheres to the counter surface, which is worn away and replenished by material adhering to the exposed counter surface [6].

The wear mechanism of PE has been related to the lubrication mode. In a study of the wear resistance of UHMWPE surfaces in joint prostheses, Wang *et al.* [6] observed that the mode of wear in joint prostheses is dependent on the nature of the motion and the effectiveness of the lubrication.

Orientation of PE at the surface can complicate the study of wear even further. In multi-directional motion wear rates increase; first orientation in the sliding direction occurs, when the motion changes direction, the oriented chain segments are loaded at an angle and the weak Van der Waals interactions are loaded rather than the strong covalent bonds in the chain direction. This generally leads to increased wear rates [6]. Over the years several options have been explored to improve the wear resistance of UHMWPE. Most of these solutions target a specific wear mechanism, but one common way to increase the wear resistance of UHMWPE, mainly effective for preventing chain orientation and the associated adhesive wear mechanism, is to cross link

UHMWPE chains using gamma irradiation, replacing the weak Van der Waals interactions with stronger covalent bonds [7]. This method is specifically of interest for UHMWPE hip cups, where multi-directional sliding combined with an adhesive wear mechanism occurs [7]. As an added bonus the gamma irradiation can be used to sterilise the UHMWPE hip cup.

Fatigue wear has been decreased by eliminating grain boundaries, since grain boundaries can be weak and facilitate crack initiation and growth [8]. Grain boundaries can be removed by sintering soft, easy to deform disentangled UHMWPE powder rather than already entangled material followed by a fast heating step that causes the chains to *explode* to their fully entangled configuration [8]. This method is especially effective for knee prostheses, where fatigue wear is the dominant wear mechanism [8].

In these two examples wear resistance is improved by changing the fabrication process to target a specific wear mechanism. In joint prostheses costs of fabrication are secondary to quality. The main issue with using UHMWPE for industrial applications is the rather laborious processing of sintering and subsequent tooling to obtain the desired final shape.

## Influence of molar mass on processing and wear

Due to the high viscosity and increased melt elasticity associated with high molar mass polymers, melt processing like injection moulding and extruding of these materials is problematic, if not impossible. However, if optimal wear resistance is required sufficient inter-chain interaction has to occur and molar masses have to be high.

The molar mass of polymers is generally characterised by the number average molar mass,  $\bar{M}_n$  the weight average molar mass,  $\bar{M}_w$  and their ratio  $D = \bar{M}_w/\bar{M}_n$ , reflecting the polydispersity, see figure 4.1A. Tervoort *et al.* have shown that, while there is a relation between wear rate and molar mass, it is neither  $M_w$ , nor  $M_n$  that shows an unambiguous correlation with the wear rate measured. They found that only the fraction above a certain molar mass sufficiently contributes to the network of physical interaction loci, e.g. entanglements, to provide wear resistance, while the lower molar mass fraction basically only represents a solvent for the high molar mass fraction, even in the solid state. This finding offers opportunities to tailor the molar mass distribution in such a way that wear resistance can also be achieved for injection mouldable parts [5].

Tervoort's reasoning can be summarised as follows: in order to effectively contribute to a network, a chain requires a minimum interaction with the other chains. This can be expressed as a number of interaction loci per chain, that can occur in crystals and in entanglements. The number of entanglements per chain also influences the number of crystals per chain, since sufficient entanglements will prevent reeling in of the chains into a single crystal during the crystallisation process [9]. In the case of PE,

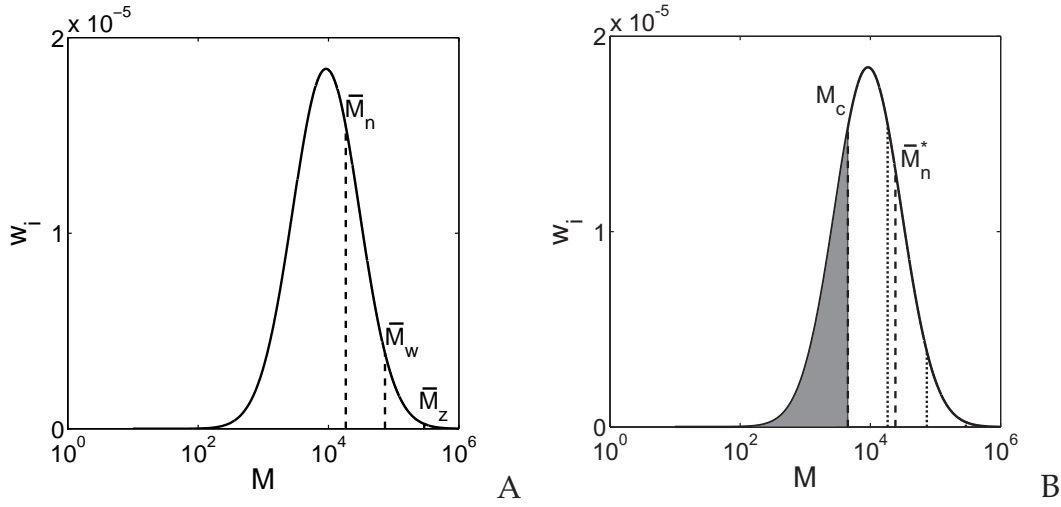


**Figure 4.1:** : Logarithmic molar mass distribution, weight fraction  $w_i$  as a function of molar mass  $M$ . Wear rate has been shown to be related to the critical molar mass for network contribution  $M_c$ , the effective number average molar mass,  $\bar{M}_N^*$ . A: The dashed lines indicate the number average molar mass,  $\bar{M}_n$ , weight average molar mass  $\bar{M}_w$  and Z-average molar mass  $\bar{M}_z$ . B: The fraction of material not contributing to the polymer network,  $1 - \phi$ , has been greyed out, the dotted lines indicate  $\bar{M}_n$ ,  $\bar{M}_w$  and  $\bar{M}_z$ , dashed lines indicate  $\bar{M}_N^*$  and  $M_c$ .

the number of entanglements,  $n_e$ , required to obtain sufficient solid state interaction loci for wear resistance was found to be between 3 and 5. Consequently the molar mass required to obtain this number of interaction loci is  $(n_e + 1)M_e$ . Chains with a molar mass below  $(n_e + 1)M_e$  have a negative effect on the strength of the network of chains and are considered to only dilute it. Tervoort *et al.* defined a set of molar mass distribution parameters to characterise the effectiveness of the semi crystalline network [5], see figure 4.1B.

The fraction of chains effectively contributing to the network can be defined as:

$$\phi = \int_{(n_e+1)M_e}^{\infty} w(M)dM \quad (4.1)$$

Where  $w(M)$  is the weight fraction of material with molar mass  $M$ . Using this value of  $\phi$ , a critical molar mass,  $M_c$ , required for an effective contribution to the network can be calculated:

$$M_c = \frac{(n_e + 1)M_e}{\phi} \quad (4.2)$$

The effective (number average) molar mass,  $\overline{M}_n^*$ , can then be defined as:

$$\overline{M}_n^* = \frac{\phi}{\int_{M_c}^{\infty} \frac{w(M)}{M} dM} \quad (4.3)$$

The number of effective interaction loci per chain,  $\overline{N}_c$  is:

$$\overline{N}_c = \frac{\phi \overline{M}_n^*}{M_e} - n_e \quad (4.4)$$

Both  $n_e$  and  $M_e$ , are considered independent of molar mass; ergo the dependence of wear rate on the molar mass distribution can be expressed as a function of  $\phi \overline{M}_n^*$  [5].

Tervoort's line of reasoning can also be used to explain the results obtained from abrasion measurements by Yang and Wu [10, 11] who found a relation between the wear rate of polymers and their strain hardening modulus. The strain hardening modulus increases with a decreasing molar mass between interaction loci, and as such with an increasing number of interaction loci per chain at comparable molar mass [12]. Indeed they found that, in accordance with Tervoort's findings, polymers with a higher strain hardening modulus exhibit a lower wear rate.

## Wear measurement methods

A wide variety of wear measurement methods is available to assess the performance of a polymers under different tribological circumstances. Most methods rely on measuring the weight loss of a polymer.

The two most frequently used methods of measuring wear are the pin-on-ring (ASTM G-77) and thrust-washer method (ASTM D-3702). In these methods a polymer sample is slid across a counter surface. With areas of both samples coming into contact repeatedly, the build up of a transfer layer can occur.

A more abrasive mechanism is studied using a pin-on-disc method (ASTM G-99-90), where a pin of the material to be characterised is slid across sandpaper in such a manner that the pin never slides across the same area of sand paper twice, preventing a transfer layer being formed in the contact area.

The micro-abrader [13, 14] is a relatively new wear measurement method. Originally designed to measure the wear resistance of coatings, it was later discovered that the method is also an excellent means of measuring a fatigue type of wear [5, 15]. Reproducibility of the results can be an issue since both the slurry composition and the loading conditions affect the results [15]. The micro abrasion experiment doesn't rely on the traditional weight loss measurement, instead wear rates are quantified by the growth of the worn area [13].



Besides this variety of macroscopic wear measurements, interest in single-asperity wear measurements has risen. Various reports exist of wear observed in FFM measurements [16–19], mainly based on the observation that under repeated loading a pattern forms in the material. Gotsmann and Dürig [19] studied this mechanism in detail and found that ridges are formed and increase in size with repeated scanning as a consequence of accumulated local strain at a length scale smaller than the radius of gyration. They argue that the ridges are formed by strain from segmental rearrangements which are immediately frozen into the glassy state within a certain time, temperature and length-scale window [19]. When this cumulative strain increases to a critical level, the material fails and wear occurs. The extremely localised nature of the processes involved is consistent with observations by Leung and Goh [18], who found no significant effect of molar mass on wear rate except for low molar mass materials.

At a microscopic, single-asperity level Hokkirigawa and Kato [20] have developed a method to quantitatively study wear in single-asperity measurements on metals. The wear volume in this method is quantified using the following equation:

$$q = A_g - A_{pu} \quad (4.5)$$

Where  $q$  is the wear volume per length of the sliding groove,  $A_g$  is the frontal area of the groove below the original surface, and  $A_{pu}$  is the frontal area of the pile up, above the original surface [21]. Since it is not uncommon for polymer scratches that  $A_{pu}$  exceeds  $A_g$  it is likely that this method will fail when applied to polymers. This will be illustrated in more detail in the results section of this chapter where the merits of this approach for single-asperity measurements on polymers are examined.

The nature of the wear has been characterised by Hokkirigawa and Kato [22] using a wear factor,

$$\xi = \frac{A_g - A_{pu}}{A_g} \quad (4.6)$$

which can vary between 0, when no wear occurs and  $A_g = A_{pu}$  and 1 when  $A_{pu} = 0$  these two extreme cases have been labelled pure ploughing and pure cutting. An intermediate wear mechanism, dubbed wedging occurs around values of  $\xi \approx 0.5$ , see table 4.1 for the ranges measured on metals. In sliding on metals these wear modes represent different wear mechanisms: cutting leads to abrasive wear, wedging is a pre-requisite for adhesive wear and if wear occurs through ploughing deformation, it is most likely through fatigue. The values in table 4.1 apply to metals.

Another single-asperity method developed at a larger scale is to scratch a material with a transparent indenter through which damage occurring in the contact can be observed in-situ using light microscopy. This method is especially successful when used to determine under which conditions cracks form and evolve [23,24].

Mechanism	Wear factor $\xi(-)$
Ploughing	0
Wedging	0.2–0.8
Cutting	0.8–1.0

**Table 4.1:** Different wear mechanisms observed in single-asperity contacts on metals defined by Hokkirigawa and Kato [22].

Material	$\bar{M}_w$ (kg/mol)	$\bar{M}_n$ (kg/mol)	$D$
UHMWPE	2000	285	7
HDPE	230	7	33
PW	2	2	1

**Table 4.2:** Molar mass characteristics of the PE grades used to develop the measurement method.

## Aim of this study

In this chapter the development and results of quantitative microscopic single-asperity wear measurements are discussed. The aim of this method is to quantitatively study the wear of PE with different molar mass distributions through repeated tribological loading of the material, and to compare the results with those obtained from micro abrader measurements by Tervoort *et al.* [5]. The advantage of using the LFA to measure wear is that only minor amounts, i.e. several micrograms, of material are required and short measurement times, between one and two minutes, suffice, the contact situation is well defined rather than a statistical distribution of local stresses and strains.

## 4.2 Materials and method

### Materials

Several grades of linear PE with different molecular weight distributions were used in the work described here.

The method, and specifically the measurement protocol, was first developed using three different PEs, an UHMWPE, an HDPE, and a polyethylene wax with a molar mass of less than  $2M_e$ , PW, see table 4.2 [25]. These PEs were compression moulded from the molten state (180 °C for 20 minutes) and subsequently annealed at 100 °C for 4 minutes after which they were embossed with a flat silicon wafer for 5 minutes at 100 °C to minimise the roughness of the samples.

Material	$\overline{M}_w$ (kg/mol)	$\overline{M}_n$ (kg/mol)	$\phi\overline{M}_n^*$ (kg/mol)	$D$
UHMWPE 610	6000	800	801.6	7.5
HDPE 7048	104.2	20.7	36.0	5.0
GUR 4012	1408.3	366.8	367.0	3.8
GHR 8110	520.1	22.7	47.2	22.9
SRM 1484	119.0	101	102.1	1.2
SRM 1483	32.1	28.9	28.9	1.1
PE MW=16,000	16.4	14.1	14.14	1.2

**Table 4.3:** Molar mass characteristics of the PE grades studied to evaluate the method developed.

Subsequently, the method developed was applied to all PEs listed in table 4.3. These samples have a thoroughly characterised molar mass distribution and were originally used in micro-abrasion experiments at the ETH in Zürich. To preserve the wear scars and crystalline structure the as received samples were not given any additional treatment to reduce the roughness. The experiments were performed at some distance from the micro-abrader wear scars to prevent possible contamination with abrasive particles trapped in the micro-abrader wear scar.

## Method

### Measurement principle

A schematic representation of the measurement protocol designed is given in figure 4.2. After applying the load, the contact is first refreshed by sliding over a distance of 100  $\mu\text{m}$ . Subsequently a reciprocating motion is made, with a sliding distance increasing with 100  $\mu\text{m}$  upon every subsequent reciprocation. Combining this motion with a high sliding velocity leads to a rapidly changing piezo excitation voltage which goes back to a reference indentation  $z(1)$  upon every reciprocation. This way the error caused by piezo creep can be quantified. After the experiment a scratch is left which shows the various stages of wear.

### The microscopic wear rate

The microscopic wear rate,  $k_\mu$  is defined as the increase of indentation  $z$  with the number of passages  $n$ . To eliminate the effect of roughness, see figure 4.3A,  $z(x, 1)$  is first subtracted from  $z(x, n)$ , see figure 4.3B. The microscopic wear rate,  $k_\mu$ , can subsequently be defined as:

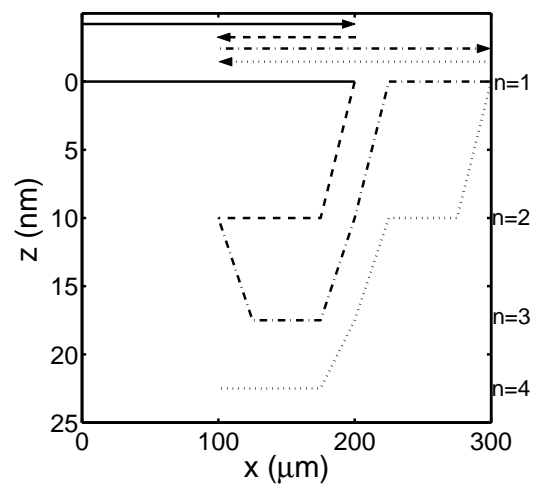


**Figure 4.2:** Schematic representation of a microscopic wear measurement. The arrows indicate the motion in the  $x$ -direction, below which is a schematic representation of the resulting tip motion. The load is applied at  $x = 0\mu\text{m}$ . To remove the effects of the initial indentation the tip is first slid across  $100\mu\text{m}$ . When the tip reaches  $100\mu\text{m}$  the measurement starts. The tip slides  $100\mu\text{m}$  in the  $x$ -direction, after which the motion is reversed and the tip slides back to the starting point of the measurement ( $x = 100\mu\text{m}$ ). Subsequently the tip is slid along the  $x$ -direction for  $200\mu\text{m}$  and back. Each subsequent reciprocating motion is  $100\mu\text{m}$  longer. The indentation increases with the number of passages  $n$ . The indentation during the first passage is taken as  $z = 0$ .

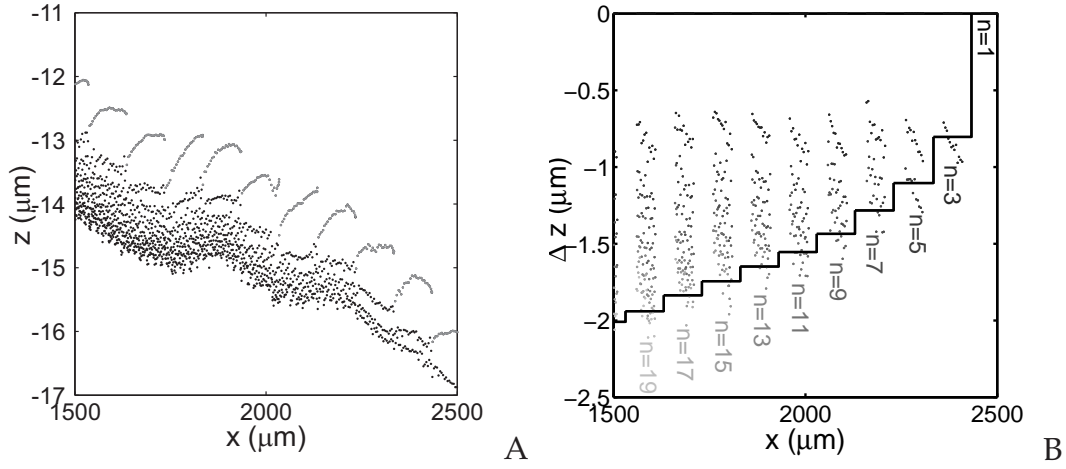


**Figure 4.3:** : Measured values of  $z$ . A: The initial signal contains information about the roughness and macroscopic slope of the sample. The grey points indicate the values measured during the first passage,  $z(x, 1)$ . B: To remove the surface roughness  $\Delta z(n)$  is determined by subtracting  $z(x, 1)$  from  $z(x, n)$ ,

$$k_{\mu}(n) = \frac{\langle z(x, 1) - z(x, n) \rangle}{n - 1} \quad (4.7)$$

where the brackets denote an average across all positions,  $x$ , along the sliding track.

### Experimental conditions

The method was developed using a diamond tip with radius  $R = 10\mu\text{m}$  and sliding velocities of 0.1, 1, 10, 100 and 1000  $\mu\text{m}/\text{s}$ . Normal loads of 2.5, 5 and 10 mN were used.

Once the method was developed, a sharper diamond tip,  $R = 5\mu\text{m}$ , was used at a sliding velocity of 750  $\mu\text{m}/\text{s}$  and with normal loads of 1, 5, 10 and 25 mN.

Both tips were spherical up to the point where the tangent reaches an angle of  $30^\circ$  to the normal direction, see figure 4.4. This means at indentations of  $z \geq 0.5R$  the indentation is proportional to the contact diameter,  $D$ , instead of to  $D^2$  for a spherical indenter.

All wear experiments were performed in fivefold.

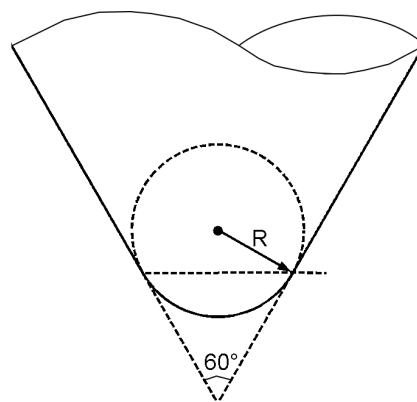


**Figure 4.4:** Schematic representation of the tip used. A diamond spherical tip of radius  $R$  mounted onto a conical titanium indenter with a conical angle of  $60^\circ$ , the indenter can be considered spherical up to an indentation of  $0.5R$  at which point the tangent of the spherical indenter equals  $60^\circ$  and the conical part of the indenter starts. Since wear measurements in this chapter sometimes exceed this maximum indentation the tip geometry and composition are accounted for. The indentation up to which the tip is spherical may deviate up to 5% from the situation sketched here.

## Additional experiments

During the development of the method Slide–Indent–Slide experiments were also performed, see section 3.2 for details on such experiments. These experiments were performed on the materials listed in table 4.2 using a tip with radius  $R = 10\mu\text{m}$ , a normal load  $F_N = 10\text{ mN}$  and velocities from 100 nm/s to 1 mm/s.

## 4.3 Results

### Development of the method

#### Slide–Indent–Slide results

During the development of the method the response of the first three different polyethylenes to tribological loading was studied under various sliding conditions using slide–indent–slide experiments, see figure 4.5. UHMWPE shows a consistent velocity weakening behaviour, the contact area grows with increasing contact age,  $\theta$ . Also, on UHMWPE the friction force is significantly higher than on the other two grades. HDPE only shows velocity weakening at high contact ages and PW shows no clear contact age effects.

The contact area,  $A$ , grows consistently with contact age for UHMWPE. For PW there is a considerable error on the deformation track measurement as wear debris obscures the edges of the contact. Since the error of the contact area measurement for PW is of the same order as the differences in contact area that were estimated, no significant effect of age on contact area could be determined. At sufficiently low sliding velocities,  $v_s < 10\mu\text{m/s}$ , HDPE also shows an increase in contact area with increasing age. However, at high sliding velocities,  $v_s > 100\mu\text{m/s}$  the contact area measured on HDPE remains constant. Around the onset of velocity weakening,  $v \approx 10\mu\text{m/s}$  ( $\theta \approx 1.5$ ), the measured contact area becomes smaller than the constant value at high sliding velocities,  $A_{c0}$ . This is phenomenologically similar to the transition to velocity strengthening observed on PS, see chapter 3.

Around the creep transition of HDPE, i.e.  $v_s \approx 10\mu\text{m/s}$ , the friction force remains constant, consequently  $\sigma_s$  slightly increases when the contact area decreases, see figure 4.5. The steady state levels of  $\sigma_s$  away from the creep transition are equal, within the experimental error. The shear stress measured on UHMWPE is significantly higher than that of the other two grades.

There is no unambiguous relation between molar mass and friction or contact area. Especially the latter is relevant for studying the wear behaviour as a function of molar mass. As a general trend the indentation during the first passage decreases with increasing molar mass. Crystallinity, and as a consequence also hardness, decreases with increasing molar mass since slow reptation, determined by the product of  $M_N$  and  $M_W$ , slows down crystallisation [9]. Since the correlation between wear rate and

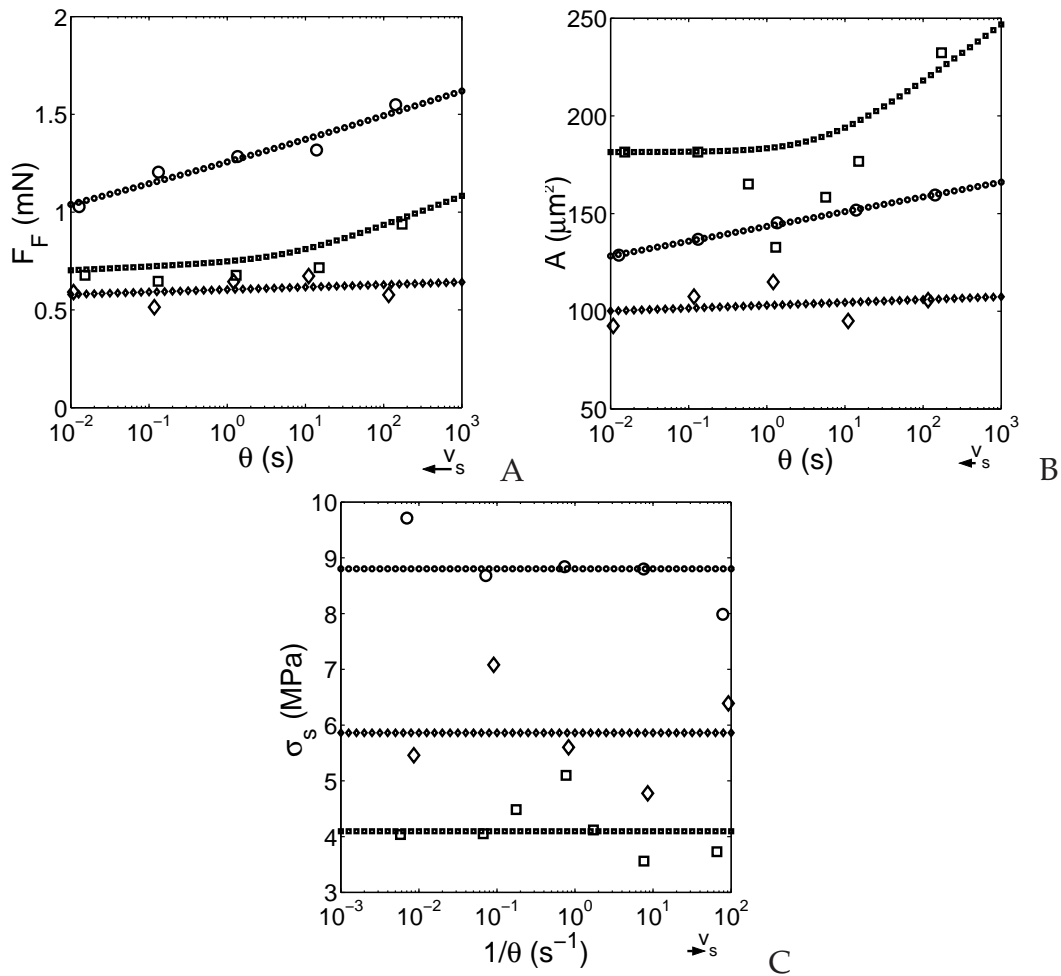


**Figure 4.5:** Friction force,  $F_F$ , contact area,  $A$ , and shear stress,  $\sigma_s$  measured in slide-indent-slide experiments on the PEs from table 4.2,  $\circ$  represents UHMWPE,  $\square$ , HDPE and  $\diamond$  PW. A:  $F_F$  as function of contact age,  $\theta$ , the lines are fits with equation 3.8. B:  $A_c$ , as a function of contact age,  $\theta$ , the lines are fits with equation 3.5. C:  $\sigma_s$ , at different deformation rates,  $1/\theta \equiv v_s$ .



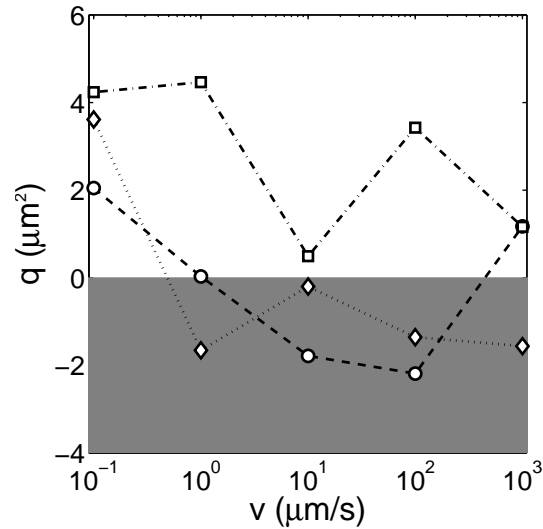


**Figure 4.6:** Wear rate  $q$ , as defined by Hokkirigawa and Kato [20], at different sliding velocities, measured at  $F_N = 10$  mN on UHMWPE( $\circ$ ), HDPE ( $\square$ ) and PW ( $\diamond$ ). Areas where  $q$  is negative are marked grey.

crystallinity has been identified as weak [5] multiple passes are required to measure wear rates.

### First pass wear quantification

An attempt was made to quantify the wear rate after a single pass from the slide-indent-slide scratches using the method developed by Hokkirigawa and Kato, see equation 4.5. The profile of the scratches was measured using an AFM. Since the volume of the ridges can be larger than that of the scratch, a negative wear rate,  $q$ , is sometimes found, see figure 4.6. Around the contact creep transition on HDPE, at  $v_s \approx 10 \mu\text{m/s}$ , the value of  $q$  for this material drops considerably.

### Transfer

It was found that material transfer, caused by strong adhesion of polymer to the diamond tip, can occur under certain sliding conditions. Since the study of material transfer is outside the focus of this study, only superficial investigation into this phenomenon was performed, i.e. limited to optimising the experimental conditions such that transfer does not affect the accuracy of the indentation measurement, since it is considered undesirable. An obvious reason is that a growing layer of polymer attached to the tip causes an error in the indentation measurement, which is used to quantify the wear rate. In figure 4.7 the conditions where transfer may occur are shown. Generally at high  $v$  and low normal forces, negative values of  $k_\mu$  were measured due to transfer. Even though positive values of  $k_\mu$  were measured on PW under

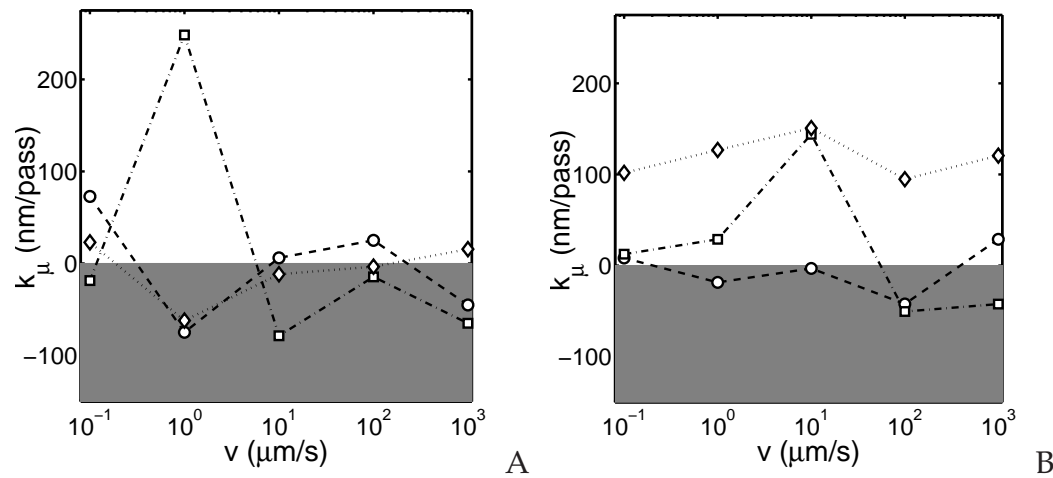


**Figure 4.7:** Wear rate,  $k_\mu$  measured during development of measurement method at various sliding velocities on polyethylenes from table 4.2 PW( $\diamond$ ), HDPE ( $\square$ ) and UHMWPE ( $\circ$ ), under normal loads of  $F_N = 2.5 \text{ mN}$  (A) and  $F_N = 10 \text{ mN}$  (B). Negative values of the wear rate (grey area) indicate possible material transfer to the tip.

all conditions, transfer occurred during measurements on this material as well, and layers of polymer attached to the apex of tip were visible under a microscope at low magnification and in some instances even with the naked eye. To see whether the Hokkirigawa and Kato quantification of wear is useful to determine the occurrence of transfer, the values of  $k_\mu$  and  $q$  have been compared, see figure 4.8A. No correlation was found between these two measures for wear at all. Since in metals transfer occurs between values of  $\xi$  between 0.2 and 0.8, the values of  $\xi$  were also compared with  $k_\mu$ , see figure 4.8B. The first thing that became apparent was that  $\xi$  could be as low as -7.5, quite different from the values between 0 and 1 given by Hokkirigawa and Kato. In order to visualise the area of interest,  $1 - \xi$  was plotted instead of  $\xi$ . Neither  $\xi$  nor  $q$  shows any correlation with  $k_\mu$ .

It was also observed that, at high normal load,  $k_\mu$  increased substantially around the onset of contact creep on HDPE. This increase in  $k_\mu$  is approximately 10 times larger than can be explained from the difference in  $z(1)$  alone. Unfortunately, as the amount of transfer could not be quantified, the effect of this transition to contact creep on transfer could not be quantified either.

From figures 4.6 and 4.7 it can be concluded that the determination of a wear rate using single-asperity experiments is certainly not trivial. While interference of transfer with the wear measurement can apparently be prevented by sliding under high normal loads at very low velocities, this is not an option for extensive wear research. One measurement of 25 passages at a sliding velocity of  $v_s = 100 \text{ nm/s}$  would take 48 hours. Experiments performed at sliding velocities above  $100 \mu\text{m/s}$  would be more practical. One possible way to achieve this appears to be to increase the contact pressure, using a sharper tip and higher normal loads.

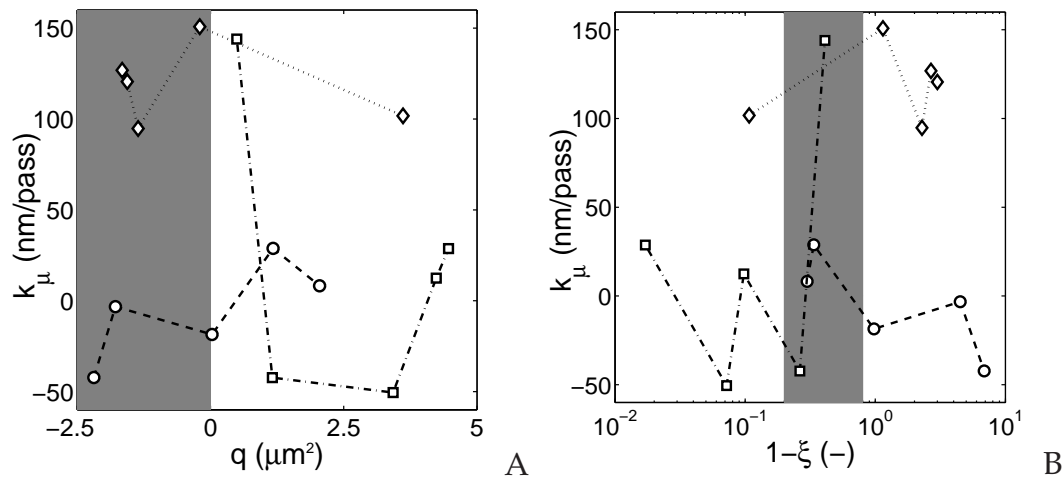


**Figure 4.8:** Wear rate,  $k_\mu$  measured at various sliding velocities on polyethylenes from table 4.2 PW( $\diamond$ ), HDPE ( $\square$ ) and UHMWPE ( $\circ$ ), under a normal load of  $F_N = 10$  mN. A comparison was made with wear volume  $q$  and wear factor  $\xi$  to determine whether a negative  $k_\mu$ , indicative of transfer, could be related to  $q < 0$  (A) or  $0.2 < 1 - \xi < 0.8$  (B). Both these conditions are indicated by grey areas.

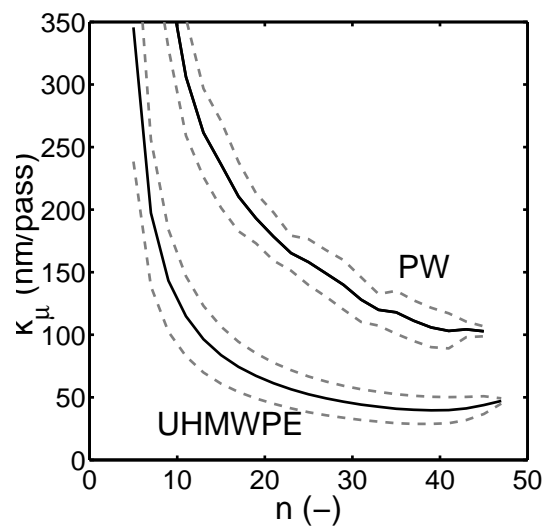


**Figure 4.9:** Wear rate  $k_\mu$  and the  $2\sigma$  errors as a function of number of passages,  $n$  calculated by applying equation 4.7 to results obtained with  $R = 10\mu\text{m}$ ,  $F_N = 10\text{mN}$  and  $v = 1$  mm/s on UHMWPE and PW.

Figure 4.9 shows the typical development of  $k_\mu$  with  $n$ , in a measurement without transfer of polymer to the tip;  $k_\mu$  decreases with  $n$  because the conformity between the tip and the groove increase as more material is worn away.

## Conclusion

Since performing an extensive range of experiments at sliding low velocities would take too long to be practical, the eventual experiments were performed using a sharper tip ( $R = 5\mu\text{m}$ ) at sliding velocities of  $v = 750\mu\text{m/s}$ . Under these conditions one measurement takes around 90 seconds and no significant effect of transfer of polymer to the tip or of piezo creep is measured.

## Results obtained using the method developed

Performing repeated sliding experiments on the PE grades from table 4.3 a fatigue type wear mechanism was aimed for, i.e. wear through repeated local straining rather than through direct cutting of the material, which can be quantified using  $q$ , see equation 4.5. Figure 4.10 shows the nature of the wear mechanism as defined, for metals, by Hokkirigawa and Kato [22]. The two grades with the lowest effective molar mass  $\phi\bar{M}_n^*$  are already worn through a cutting mechanism during the first passage, indicated by the high values of  $\xi$ . Another interesting observation is that at low loads,  $F_N = 1\text{ mN}$   $\xi$  appears to increase with  $\phi\bar{M}_n^*$  within the wedging range, except for the lowest molar mass material S10 which shows cutting wear under all loads. At higher loads  $\xi$  drops for all materials except S9 and S10, the two materials with the lowest molar masses. In cases where  $\xi$  is smaller than 0.8,  $q$  is small indicating that no substantial wear occurred during the first passage in those experiments.

For the conditions under which cutting was observed a strong correlation between  $q$  and the frontal contact area,  $A_f$  was found, see figure 4.11. It was found that  $q = 0.37A_f$  under all conditions except for  $F_N = 1\text{ mN}$ . Under higher loads the spherical diamond part of the indenter is completely pressed into the material and the supporting titanium cone is also in contact.

The microscopic wear rate,  $k_\mu$ , is indeed lower for higher values of  $\phi\bar{M}_n^*$ , see figure 4.12. The data could be fitted with a linear relation between  $\phi\bar{M}_n^*$  and  $k_\mu^{-1}$ , equivalent to the macroscopic relation between  $\phi\bar{M}_n^*$  and  $k^{-1}$  Tervoort *et al.* found [5]. Although the values of  $\xi$  suggest that both direct cutting and fatigue wear occurred, this doesn't appear to affect the correlation between  $\phi\bar{M}_n^*$  and  $k_\mu^{-1}$ .

When the results are compared to the macroscopic values measured on the same samples using a micro-abrader at the ETH in Zürich a linear correlation exists. The correlation coefficients,  $R^2$ , between  $k_\mu$  and  $k$  are 0.79, 0.87, 0.97 and 1.00 for  $F_N = 1, 5, 10$  and  $25\text{ mN}$  respectively, see figure 4.13. Good fits could be drawn using  $k_\mu = a_F(F_N) + bk$ , with  $a_F$  the offset for  $k_\mu$  where  $k = 0$ . The value of  $a_F$  goes towards

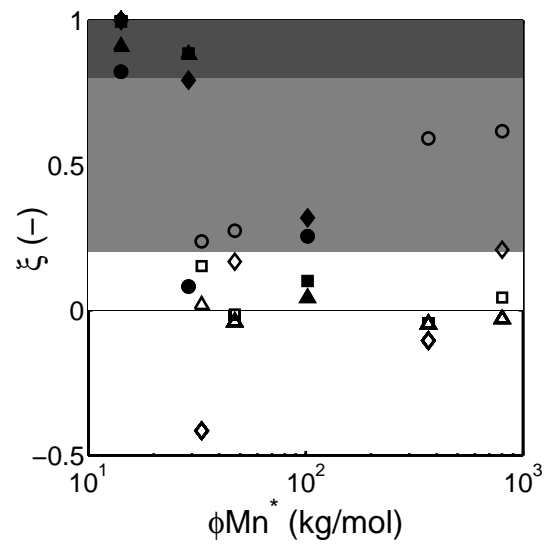


**Figure 4.10:** Wear factor  $\xi$  as a function of effective molar mass  $\phi\bar{M}_N^*$  for different normal forces:  $F_N = 1$  mN ( $\circ$ ),  $F_N = 5$  mN ( $\triangle$ ),  $F_N = 10$  mN ( $\square$ ) and  $F_N = 25$  mN ( $\diamond$ ). Closed symbols indicate materials with a narrow molar mass distribution. The grey areas indicate the wedging and cutting range for metals, as defined in table 4.1.

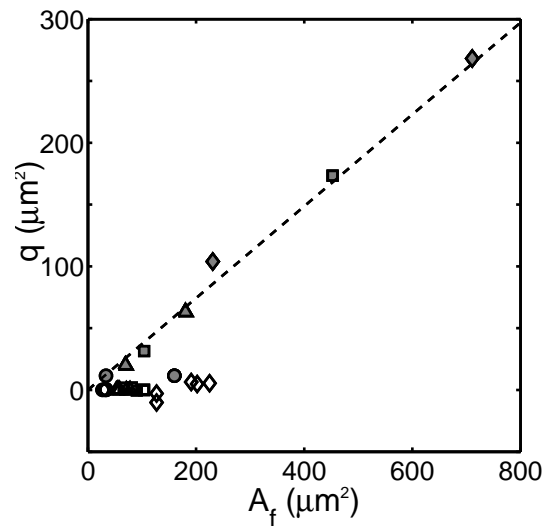


**Figure 4.11:** Hokkirigawa and Kato wear rate  $q$  as a function of estimated frontal contact area  $A_f$  for different normal forces:  $F_N = 1$  mN ( $\circ$ ),  $F_N = 5$  mN ( $\triangle$ ),  $F_N = 10$  mN ( $\square$ ) and  $F_N = 25$  mN ( $\diamond$ ). Grey symbols indicate a cutting wear mechanism was observed, these data were fitted with  $q = 0.37A_f$  (line).

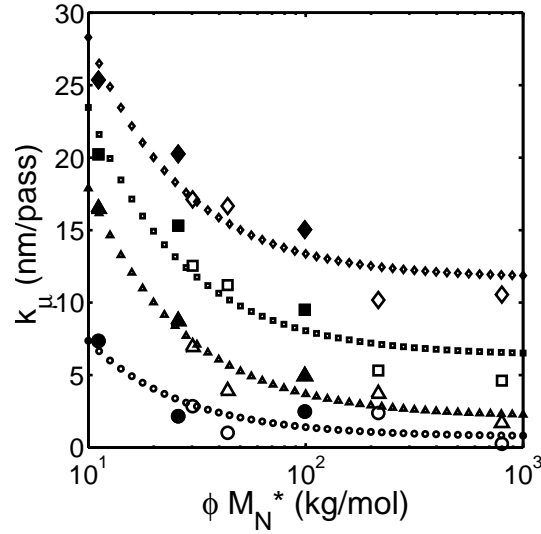


**Figure 4.12:** Wear rates,  $k_\mu$  as a function of effective molar mass  $\phi\bar{M}_N^*$  for different normal forces:  $F_N = 1$  mN ( $\circ$ ),  $F_N = 5$  mN ( $\triangle$ ),  $F_N = 10$  mN ( $\square$ ) and  $F_N = 25$  mN ( $\diamond$ ). Closed symbols indicate materials with a narrow molar mass distribution.

0 with increasing contact loads, see figure 4.14. Data could be fitted using  $b = 4.86$  N/m·pass.

Wear rate  $q$  and wear rate  $k_\mu$  are indicators for two wear mechanisms, abrasive and fatigue wear, respectively. Both can be measured using the LFA. In the LFA experiments performed in this chapter little effect of molar mass on  $q$  was observed, only the two PE grades with the lowest molar masses showed significant abrasive wear. The occurrence of abrasive wear appears to be an on/off event, i.e. below some critical molar mass it occurs, at a wear rate independent of molar mass, above this critical molar mass no significant abrasive wear occurs. This transition appears to take place around  $\phi\bar{M}_n^* = 30$  kg/mol. The wear rate  $q$  is proportional to the frontal area of the contact, see figure 4.11. Fatigue wear occurs after several passages, wear rate  $k_\mu$  increases linearly with increasing  $\phi\bar{M}_n^*^{-1}$ , similar to the dependence of the macroscopic wear factor  $k$  on  $\phi\bar{M}_n^*^{-1}$  observed by Tervoort *et al.* on a micro-abrader. Here too a critical molar mass can be observed. However, this molar mass is not absolute, as in abrasive wear, but dependent on the contact mechanics. From the linear relation between  $k_\mu$  and  $k$  a critical molar mass, above which fatigue type wear is minimal, can be determined. This is illustrated in figure 4.13B. Since  $k$  is proportional to  $\phi\bar{M}_n^*^{-1}$ , the higher  $-a_F(F_N)$  is, the lower the critical molar mass will be, in case of  $F_N = 1$  mN and an  $R = 5$   $\mu$ m radius tip, this critical molar mass is around  $\phi\bar{M}_n^* \approx 35$  kg/mol. For  $F_N = 5$  mN the corresponding molar mass would become so high that PE of any molar mass would show fatigue wear.

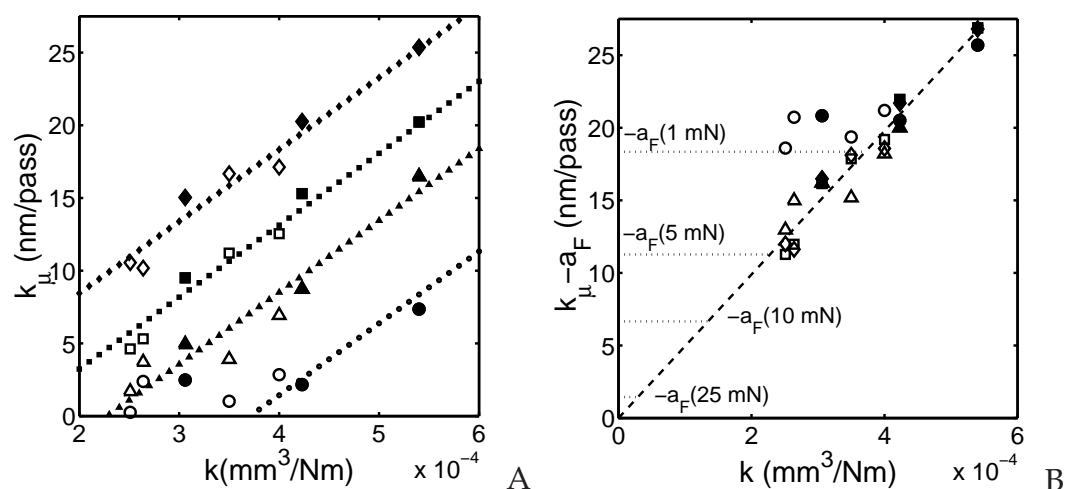


**Figure 4.13:** Microscopic wear rate,  $k_\mu$ , at normal loads of 1 ( $\circ$ ), 5 ( $\triangle$ ), 10 ( $\square$ ), and 25 ( $\diamond$ ) mN plotted against the macroscopic wear rate,  $k$ , measured using a micro-abrader. Closed symbols indicate the grades with a narrow molar mass distribution. A: Measured values, dotted lines indicate the best fit with an identical slope for all normal forces. B: Values of the microscopic wear rate shifted by  $a_F$ , plotted against the values of  $k$  measured by Tervoort *et al.*.

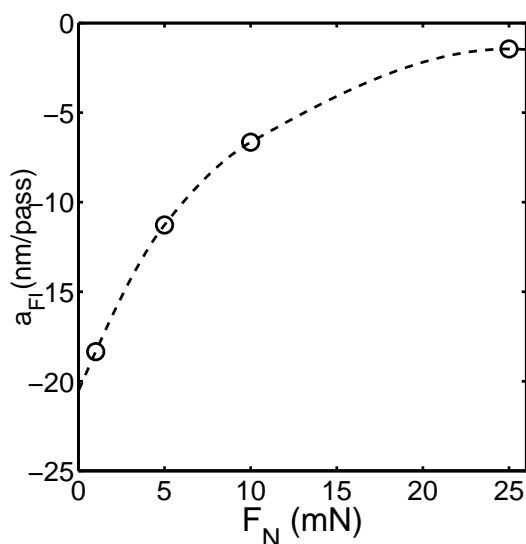


**Figure 4.14:** Shift factor  $a_F$  as a function of normal load  $F_N$ , determined from a linear fit between  $k$  and  $k_\mu$ .

## 4.4 Conclusion

A microscopic single-asperity method for quantitative measurement of the wear resistance of polymers was developed. The abrasive and fatigue wear resistance of a polymer can be quantitatively measured using a single asperity technique provided that no transfer of polymer to the tip occurs. To achieve transfer free conditions at high sliding velocities the tip has to be sufficiently sharp. A tip radius of  $R = 5\mu\text{m}$  was found to be sharp enough at normal loads between  $F_N = 1\text{ mN}$  and  $F_N = 25\text{ mN}$  and sliding velocities of  $v_s = 750\ \mu\text{m/s}$ .

The advantage of using the LFA to measure wear is that only minor amounts, i.e. several micrograms, of material are required and short measurement times, between one and two minutes, suffice. Well defined contacts can be used to quantify wear in a manner, apparently representative of a micro-contact in a micro-abrader experiment, opening up possibilities for the quantitative study of fatigue wear of polymers in terms of local stresses and strains.

A correlation between the microscopic wear rate,  $k_\mu$ , and molar mass was found using the same definition of molar mass as used by Tervoort *et al.* [5]. A strong linear correlation is found between the values of  $k_\mu$  measured using the LFA and the values of  $k$  measured using a micro-abrader when a sufficiently high normal load and a sharp tip are used in the LFA experiments. This correlation becomes stronger at increasing normal load. When the normal load is reduced sufficiently, the molecular weight required to obtain optimal wear resistance decreases.

During the first passage abrasive wear could be quantified using the method defined by Hokkirigawa and Kato. The abrasive wear rate  $q$  was found to be proportional to the frontal area of the contact and only occurred below a certain critical molar mass.



## References

- [1] Steijn, R. P. (1986). Failure of plastics. pages 357–392. Hanser Publishers Munich.
- [2] Lemstra, P. J., Bastiaansen, C. W. M., Peijs, T. and Jacobs, M. J. N. (2000). Fibres based on ultra-high molecular weight polyethylene – processing and applications. In Ward, I. M., Coats, P. D., Dumoulin, M. M., editors, *Solid Phase Processing Of Polymers*, pages 172–213. Carl Hanser Verlag.
- [3] Pooley, C. M. and Tabor, D. (1972). Friction and molecular structure: the behavior of some thermoplastics. *Proc. Roy. Soc London, Ser. A*, **329**, 251–274.
- [4] Wheeler, D. R. (1981). The transfer of polytetrafluoroethylene studied by x-ray photoelectron spectroscopy. *Wear*, **66**, 355–365.
- [5] Tervoort, T. A., Visjager, J. and Smith, P. (2002). On abrasive wear of polyethylene. *Macromolecules*, **35**, 8467–8471.
- [6] Wang, A., Essner, A., Polineni, V. K., Stark, C. and Dubleton, J. H. (1998). Lubrication and wear of ultra-high molecular weight polyethylene in total joint replacements. *Tribol. Int.*, **31**, 17–33.
- [7] Yamamoto, K., Masaoka, T., Manaka, M., Oonishi, H., Clarke, I., Shoji, H., Kawanabe, K. and Imakilre, A. (2004). Micro-wear features on unique 100-Mrad cups: Two retrieved cups compared to hipsimulator wear study. *Acta Orthop. Scand.*, **75**, 134–141.
- [8] Rastogi, S., Kurelec, L., Lippits, D., Wimmer, M. and Lemstra, P. J. (2005). Novel route to fatigue-resistant fully sintered ultrahigh molecular weight polyethylene for knee prosthesis. *Biomacromolecules*, **6**, 942–947.
- [9] Hoffman, J. D. and Miller, R. L. (1997). Kinetics of crystallization from the melt and chain folding in polyethylene fractions revisited: theory and experiment. *Polymer Papers*, **38**, 3151–3212.
- [10] Yang, A. C.-M. and Wu, T. W. (1993). Abrasive wear and craze breakdown in polystyrene. *J. Mat. Sci.*, **28**, 955–962.
- [11] Yang, A. C.-M. and Wu, T. W. (1997). Wear and friction in glassy polymers: Microscratch on blends of polystyrene and poly(2,6-dimethyl-1,4-phenylene oxide). *J. Pol. Sci. B*, **35**, 1295–1309.
- [12] van Melick, H. G. H., Govaert, L. E. and Meijer, H. E. H. (2003). On the origin of strain hardening in glassy polymers. *Polymer*, **44**, 2493–2502.
- [13] Rutherford, K. L. and Hutchings, I. M. (1997). Theory and application of a micro-scale abrasive test. *J. Testing Eval.*, **25**, 250–260.
- [14] Gee, M. G., Grant, A. J., Hutchings, I. M., Kusano, Y., Schiffman, K., Van Acker, K., Poulat, S., Gachon, Y., von Stebut, J., Hatto, G. and Plint, G. (2005). Results from an interlaboratory exercise to validate the micro-scale abrasion test. *Wear*, **259**, 27–35.
- [15] Mergler, Y. J. and Huis in 't Veld, A. J. (2003). Micro-abrasive wear of semi-crystalline polymers. In Dalmaz, G. and Lubrecht, A., editors, *Tribological Research and Design for Engineering Systems: Proceedings of the 29th Leeds-Lyon Symposium on Tribology held In Leeds, UK 3rd–6th September 2002*, Tribology and Interface Engineering Series, pages 165–173, Amsterdam, 2003. Elsevier.

- [16] Aoike, T., Uehara, H., Yamanobe, T. and Komoto, T. (2001). Comparison of macro- and nanotribological behavior with surface plastic deformation of polystyrene. *Langmuir*, **17**, 2153–2159.
- [17] Aoike, T., Yamamoto, T., Uehara, H., Yamanobe, T. and Komoto, T. (2001). Surface deformation properties of polystyrene as evaluated from the morphology of surfaces scratched by using the tip of a scanning force microscope. *Langmuir*, **17**, 5688–5692.
- [18] Leung, O. M. and Goh, M. C. (1992). Orientational ordering of polymers by atomic force microscope tip-surface interaction. *Science*, **255**, 64–66.
- [19] Gotsmann, B. and Dürig, U. (2004). Thermally activated nanowear modes of a polymer surface induced by a heated tip. *Langmuir*, **20**, 1495–1500.
- [20] Hokkirigawa, K. and Kato, K. (1988). The effect of hardness in the transition of the abrasive wear mechanism of steels. *Wear*, **213**, 241–251.
- [21] Masen, M. A., de Rooij, M. B. and Schipper, D. J. (2005). Micro-contact based modelling of abrasive wear. *Wear*, **258**, 339–348.
- [22] Hokkirigawa, K. and Kato, K. (1989). Theoretical estimation of abrasive wear resistance based on microscopic wear mechanism. In *Proceedings of the 7th International Conference on Wear of Materials*, pages 1–8. American Society Of Mechanical Engineers.
- [23] Bles, M. H., Winkelman, G. B., Balkenende, A. R. and den Toonder, J. M. J. (2000). The effect of friction on scratch adhesion testing: application to a sol-gel coating on polypropylene. *Thin Sol. Films*, **359**, 1–13.
- [24] Chateauinois, A. and Briscoe, B. J. (2003). Nano-rheological properties of polymeric third bodies generated within fretting contacts. *Surf. Coat. Techn.*, **163–164**, 435–443.
- [25] Schaake, R. P., den Toonder, J. M. J., Vellinga, W. P. and Meijer, H. E. H. (2005). One minute wear rate measurement. *Macromol. Rap. Comm.*, **26**, 188–191.



# Conclusions and recommendations

---

## 5.1 Conclusions

In this thesis the results obtained from tribological microscopic single-asperity measurements are described. The study focussed on the effect of molar mass on friction and wear.

The single-asperity measurements were performed using the LFA, a microscopic single-asperity friction measurement device. The LFA can measure indentation, friction force, sliding velocity, tip position and normal force simultaneously. It also allows for experimentation across 5 orders of magnitude in sliding velocity and relatively complex sliding motion protocols. The large range of sliding velocities allows for a quantitative prediction of stick-slip from steady-state measurements.

By combining slide-indent-slide measurements with rate-and-state equations shear stress and contact area effects can be distinguished. Polystyrenes of two different molar masses, but with similar bulk glass transition temperatures, were subjected to this combination of measurements and analysis. The contact area was expected to be related to the bulk properties and the shear stress was expected to be related to the surface properties. The friction force was found to be higher for the high molar mass polystyrene, this could be attributed to shear stress effects, since during steady state sliding the contact area was independent of molar mass. During hold the lower molar mass polystyrene showed more creep, leading to a larger contact area, and higher friction, upon resuming sliding. The shear stress relaxation could be quantified using the same fit parameters independent of molar mass. The dissipative mechanism was quantitatively identified as a delta-relaxation for the higher of the two molar masses used, for the lower molar mass experiments at a higher sliding velocities or elevated temperatures would be required to determine the dissipative mechanism in order to obtain a stress effect sufficiently strong to quantify.

Slide-indent-slide experiments were also performed on polyethylene, an UHMWPE,

an HDPE and a PE wax. The velocity dependence of the friction force on PE could also be described from analysis using the rate-and-state equations. Unlike the measurements on PS no significant increase of shear stress with sliding velocity was observed. On the contrary, the shear stress on UHMWPE appeared to decrease with increasing sliding velocity, for PE wax the friction force was found to be independent of the sliding velocity, HDPE showed velocity weakening at low sliding velocities and UHMWPE showed velocity weakening throughout the sliding velocity range.

A microscopic single-asperity wear measurement method was developed which could be used to quantitatively measure both abrasive and fatigue wear in one measurement. During the first passage abrasive wear is measured. During subsequent passages a fatigue type wear mechanism occurs. The increase of indentation with number of passages shows a linear correlation with micro-abrader measurements. The relation between wear rate and molar mass differed between abrasive and fatigue wear. Above a certain molar mass no abrasive wear occurs. The fatigue wear rate shows a less abrupt relation with molar mass, the higher the effective molar mass  $\phi\bar{M}_n^*$ , the more resistant a polymer is to fatigue wear. From comparing micro-abrader and LFA wear measurements, a microscopic contact condition can be defined where fatigue type wear is minimal above a certain effective molar mass  $\phi\bar{M}_n^*$ .

The microscopic fatigue wear measurements described in chapter 4 allow for a study of polymer wear in which not only the wear rate as a function of material properties can be studied but also the local contact conditions leading to that wear mechanism can be quantified. This way, a road is opened to study the wear in terms of local stress-strain distributions and the intrinsic and failure behaviour of the material. In contrast to what can be achieved using a stochastic approach such as with a micro abrader.

## 5.2 Recommendations

There are a couple of recommendations that can be made regarding single-asperity research with the objective to study the influence of polymer properties on tribological behaviour. To be able to measure across several orders of magnitude of sliding velocities is perhaps the most important prerequisite, as is illustrated in chapter 3. It is just as important that the contact area can be quantitatively determined. Where in chapter 3 the work relied on one central assumption concerning the size of the contact area, i.e. the contact diameter being equal to the distance between the summits of the pile-up left after the experiment, a more direct measurement of the contact area is of course desired. At the microscopic scale this can be achieved optically, but when going to smaller contact diameters this will no longer suffice. An absolute measurement of the indentation, rather than relative as is currently the case with the LFA, would remove the need for post-factum measurement of the contact area. To achieve this, the separation of lateral and normal displacement measurement currently used in the LFA offer a good starting point. The downside of the current method is its

fragility; leafspring units of sufficient linearity and fatigue resistance are difficult to manufacture and the focus error measurement system, although still an accurate way to measure the displacements, is no longer produced. The most critical component with regard to the indentation measurement is the use of a piezo for normal direction displacement, using a linear system, with a linear displacement measurement, instead would be highly recommended. It also becomes apparent from the results in chapter 3 that even 5 orders of sliding velocity do not guarantee all velocity effects will be measured. A time–temperature superposition method allowing for measurements at both higher and lower temperature would be preferable to the current limitation of only being able to work at ambient conditions. In whatever direction the experimental opportunities are improved, reliability should not be let out of sight, as well as the time and effort it takes to prepare an experiment.

With regard to wear measurements a lot of opportunities are still open. In chapter 4 it has been illustrated that microscopic single–asperity wear measurements can offer a lot of information, especially if combined with macroscopic measurements. The potential of the experiments described in chapter 4 has been far from fully explored; it should be possible to calculate local strains, but again an absolute indentation measurement would be required instead of a measurement of indentation relative to some reproducible reference situation. Also, in view of the time available, not the complete sliding track was examined, only the  $n = 1$  part of the scratch was examined post–factum, the  $n = 3$  to  $n = 49$  scratches doubtlessly contain much further information. It should be possible to determine a local strain–fatigue wear relation, as well as to relate this to the molar mass distribution. Polyethylene is of course only one of many polymer materials and the effect of stronger chain interaction, e.g. through hydrogen bridges, is another line of investigation that, with the right combination of techniques, could lead to valuable information.

Another interesting exercise would be to dissolve lubricant in a polymer. How does it affect the network, the contact area and the shear stress? How does this affect adhesion, something avoided with great care and sometimes great effort in the work presented in this thesis. How can adhesive effects be quantified and the tip subsequently be easily replaced or cleaned? How can measurements involving adhesive contacts be reproduced? These are all challenging questions which are both of scientific interest and will provide a bridge to the world of applied science.

Whatever measurements are performed on the LFA, a good model needs to support the results. One of the issues that will be most challenging is the thickness and of the shear layer and the effects of chain ends and surface loops in this layer.

The LFA was designed to work on a meso–scopic scale, a somewhat ambiguous denomination meaning in between, it seems it is truly acting on this *meso* scale, results obtained with it can be linked with FFM, nano–indentation, macroscopic fatigue wear and macroscopic friction results.



# Samenvatting

---

Het kwantificeren en begrijpen van wrijving en slijtage in termen van materiaaleigenschappen is, vooral in het geval van materialen met tijd- en temperatuursafhankelijke eigenschappen, zoals polymeren, niet eenvoudig. In dit proefschrift ligt de nadruk op kwantitatieve meettechnieken die kunnen worden benut om wrijving en slijtage van kunststoffen te beschrijven.

Om de invloed van materiaaleigenschappen op wrijving en slijtage te begrijpen is het nodig in te zoomen op de relevante processen in een glijdend contact. Een macroscopisch contact tussen twee oppervlakken bestaat normaal gesproken uit meerdere micro-contacten tussen ruwheidstoppen. Deze micro-contacten vormen samen het werkelijke contactvlak, waarvan de omvang afhankelijk is van de materiaaleigenschappen van beide oppervlakken alsmede de belasting die hierop wordt uitgeoefend. De wrijvingskracht die experimenteel gemeten wordt is het produkt van dit ware contactoppervlak en een gemiddelde effectieve afschuifspanning.

Omdat het ware contactoppervlak moeilijk te beïnvloeden en kwantificeren is in macroscopische contacten, zijn dergelijke contacten niet geschikt om oppervlakten en afschuifspanningseffecten van elkaar te onderscheiden. Dit in tegenstelling tot *Single-Asperity* contacten, waar het werkelijke en schijnbare contactoppervlak even groot zijn en dus de mogelijkheid bestaat het ware contactoppervlak te beïnvloeden en kwantificeren.

In het werk dat in dit proefschrift worden metingen aan microscopische *Single-Asperity* contacten gebruikt om relaties tussen variaties in materiaal en tribologische eigenschappen te bepalen. Deze metingen zijn uitgevoerd met de LFA, of *Lateral Force Apparaat*. Het oorspronkelijke ontwerp van dit apparaat is aangepast om de doelstellingen van dit onderzoek beter te kunnen verwezenlijken. Een nieuwe aandrijving, ontwikkeld om over 5 ordegroottes van glijnsnelheid te kunnen meten in combinatie met een nauwkeurige positiebepaling maakt het mogelijk *Single-Asperity* metingen bij sterk verschillende snelheden uit te voeren, hiervan is aangetoond dat dit van belang is om wrijvingsmetingen aan kunststoffen te interpreteren. De positiebepaling is met name van belang bij de ontwikkeling van slijtage metingen.

Bij metingen aan wrijving in een glijdend contact is het maken van onderscheid tussen de effectieve afschuifspanning en het ware contactoppervlak van cruciaal be-



lang. Afhankelijk van mechanische eigenschappen en experimentele condities vertonen alle materialen kruip op een karakteristieke tijdschaal. In kunststoffen is kruip in het bijzonder van interesse aangezien de bijbehorende tijdschalen relatief kort zijn. In *Single-Asperity* wrijving bepalen de glij snelheid en de radius van de tip de belastingsduur van het oppervlak. Dit bepaalt hoeveel kruip er optreedt en derhalve hoe groot het contactoppervlak is. In dit proefschrift wordt aangetoond dat het effect van contactoppervlak onderscheiden kan worden van dat van de afschuifspanning door gebruik te maken van *Single-Asperity* technieken over een groot bereik van snelheden.

Bij het bestuderen van relaties tussen materiaaleigenschappen en slijtage vormen de vele microcontactjes in macroscopische contacten een experimentele drempel aangezien deze een grote variatie in mate van deformatie vertonen. Een veel genoemde materiaaleigenschap die van belang zou zijn voor slijtage is de deformatie bij falen, wanneer de mate van deformatie grote variaties vertoont is dit echter lastig aan te tonen. In een studie aan PE waarbij gebruik wordt gemaakt van een *Single-Asperity* techniek wordt een verband tussen slijvastheid en molgewichtsverdeling aangetoond.

Kwantitatieve *Single-Asperity* metingen zijn een onmisbare stap in het begrijpen en beschrijven van relaties tussen structuur en tribologisch gedrag. Waar macroscopische tribologische experimenten op de oppervlakte blijven kunnen *Single-Asperity* technieken gebruikt worden om dieper te graven.

# Dankwoord

---

Graag wil ik hier iedereen bedanken die op een of andere manier in de afgelopen jaren heeft geholpen mij te motiveren, te inspireren, af te leiden of anderszins zijn of haar invloed heeft gehad op dit proefschrift.

Allereerst wil ik mijn directe begeleiders bij de TU/e hartelijk bedanken. Willem-Pier Vellinga zijn niet aflatende enthousiasme, kritische houding en vermogen te inspireren zijn belangrijke steunpilaren geweest in de tot stand koming van dit werk. Ik wil Han Meijer bedanken voor de mogelijkheid dit onderzoek binnen zijn groep uit te voeren en het vertrouwen dat hij mij hierin geschonken heeft. Tot slot heeft Jaap den Toonder sinds zijn aanstelling als deeltijdhoogleraar met een aanstekelijk enthousiasme en zijn ervaring op het gebied van contactmechanica de nodige positieve bijdragen aan dit onderzoek geleverd. Het Dutch Polymer Institute wil ik bedanken voor het financieren van dit onderzoek.

Dit werk was onmogelijk geweest zonder de ondersteuning van Toon Hoeben en Marc van Maris op het Multi-Scale lab. Erwin Dekkers, Simon Plukker en Rinus Janssen van de GTD wil ik hartelijk bedanken voor de ontwikkeling, verbetering en ondersteuning rond de LFA. Zonder hen waren de experimentele resultaten in dit proefschrift niet mogelijk en van een dergelijke hoogstaande kwaliteit geweest. Ook Otto van Asselen, Joachim Loos, Pauline Schmit, Kees Meesters, Harry van Leeuwen, Hans van Griensven, Patrick van Brakel, Leo Wouters, Ine de Lepper, Monique Sosef, Iris Brakman, Germaine Geerts, Yvon Biemans, Alice van Litsenburg hebben de nodige ondersteuning verschaft. Marleen Rieken wil ik bedanken voor de jarenlange ondersteuning, met name de uitstekende hulp bij het rondkrijgen van de laatste zaken.

Door de jaren heen hebben mijn verschillende kamergenoten, Hedzer de Boer, Marcel Meeuwissen, Maurice van der Beek, Alexander Sarkissov, Stephen Onraet, Raoul van Loon, Marco van den Bosch en Alpay Aydemir, Edwin Smit, Emile van der Heijde en Henk Slot allemaal een positief effect gehad op de werksfeer. Evenals mijn overige collegae, met name Vinayak Khatavkar, Ruchi Rastogi, Peter Janssen, Jan-Willem Housmans, Abdul Matin, Roel Janssen, Alexander Zdravkov, Jesus Mediavilla, Sebastiaan Boers, Hans van Dommelen, Bernard Schrauwen, Berent Wolters, Reinder Roos, Isle van Casteren, Bert Keestra, Harold van Melick, Jules Kierkels, Christophe Pelletier, David Trimbach, Edwin Klompen, Edwin Gelinck, Cor Lossie,

Jan-Paul Krugers, Bert Dillingh, Bastiaan Krosse, Ben Boerstoel, Jan Breen en Hartmut Fischer.

Yvonne Mergler wil ik hartelijk bedanken voor haar collegialiteit, vriendschap en morele ondersteuning. Het gesprek met haar waarin het idee grip kreeg om aan een promotieonderzoek te beginnen zal ik nooit vergeten; het heeft ingrijpende gevolgen gehad.

Uiteraard was dit werk onmogelijk geweest zonder de noodzakelijke afleiding. De bandleden Wilbert van den Eijnde, Marco van der Linde, Corné Rentrop, Greg Alcott en Marc Koetse, ben ik grote dank verschuldigd voor de vele uren Rock & Roll. Frank Grob, Dani Bortz, Hans Linden, Ursula Meijer, Jasper Michels, Ross Archer, en vele anderen wil ik bij dezen bedanken voor het mede nuttigen van bier en overige versnaperingen. Edwin Stam wil ik bedanken voor zijn onbegrensde sociaalheid, een steun en toeverlaat bij kopzorgen en huishoudelijke problemen. Kornel Hoekerd, Marc van Rossum, Arjan Hoornstra, Michel Bleeker, Boudewijn Eindhoven en Marion van Wezel, jullie vriendschap was onontbeerlijk.

Tot slot een woord van dank richting mijn familie. Mijn ouders, opa, Michel, Liedeke, Ella en Lori zijn er altijd voor mij en ik hoop dat we nog lang op elkaar kunnen rekenen.

Richard Schaake

Nieuwegein, 7 Juni 2006

# Curriculum Vitae

---

Richard Schaake (Apeldoorn, September 10<sup>th</sup> 1973) started studying Analytic Chemistry at the Rijkshogeschool IJsselland in 1990. After a year he switched to materials technology for which he got his Bachelors degree in 1996. In 1997 he started working in the Tribology group at TNO. In 2001 he was offered the opportunity to pursue a PhD-degree within the Materials Technology group at the Technical University of Eindhoven. During this period he also followed RPK courses on polymer chemistry, physics, properties, rheology and processing. The results of this work are presented in this thesis. In 2006 he started working as a polymer engineer within the SKF Research and Development Company.



# List of publications by Richard Schaake

---

R.P. Schaake, J.M.J. den Toonder, W.P. Vellinga and H.E.H Meijer, *One Minute Wear Rate Measurement* In: *Macromolecular Rapid Communications* 26 (2005) pp. 188-191

R.P. Schaake, W.P. Vellinga and H.E.H. Meijer, *Microtribology of monodisperse polystyrene* In: Ed. G. Dalmaz, *Transient processes in tribology - Proceedings of the 30th Leeds-Lyon Symposium on tribology 2003* Elsevier, Amsterdam (2004) pp. 507-516

Y.J. Mergler and R.P. Schaake, *Relation between strain hardening and wear resistance of polymers* In: *Journal of Applied Polymer Science* 92 (2004) pp. 2689-2692

Y.J. Mergler R.P. Schaake and A.J. Huis in't Veld, *Material transfer of POM in sliding contact* In: *Wear* 256 (2004) pp. 294-301

Y.J. Mergler, R.J. van Kampen, W.J. Nauta, R.P. Schaake, B. Raas J.G.H. v Griensven and C.J.M. Meesters, *Influence of yield strength and toughness on friction and wear of polycarbonate* In: *Wear* 258 (2004) pp. 915-923

R.P. Schaake, E. van der Heide and A.J. Huis in't Veld, *Tools for unlubricated sheet metal forming* In: Ed. H.J.J. Kals et al., *Sheet Metal 1998 - Proc. Of the 6th International Conference held at the Univ. Twente, The Netherlands 6-8 April 1998* Universiteitsdrukkerij Twente, Enschede (1998) pp. I-323 - I-332

R.P. Schaake, W.P. Vellinga and H.E.H. Meijer *Molecular weight effects in quantitative microscopic single asperity friction on PS* submitted to *Tribology Letters*

R. P. Schaake, W. P. Vellinga, J. M. J. den Toonder and H. E. H. Meijer: *Quantitative microscopic study of fatigue-type wear on PE*, in preparation